中国激光

多场调控金属激光增材制造研究现状与展望

高海瑞，李继康，张振武，郑可盈，向泓澔，魏青松*

华中科技大学材料科学与工程学院，湖北 武汉 430074

摘要 激光增材制造可实现高性能金属复杂构件整体化成形，在航空航天、汽车、医疗等领域具有广阔应用前景。但是，高斯激光作用产生不均匀温度场、极高的温度梯度以及不稳定的流场，导致飞溅、球化、气孔、残余应力和裂纹等缺陷及各向异性的微观性能，影响了该技术更广泛的应用。光束矫形和场辅助原位调控激光增材制造过程是控制缺陷产生的有效方法。综述了国内外在光束矫形以及热、磁和超声多场调控金属激光增材制造领域的研究进展，重点揭示外场-激光-材料-组织-性能间的作用机理，并对多场调控金属激光增材制造未来发展进行了展望，可为金属激光增材制造的高性能调控提供有益参考。

关键词 激光技术；激光增材制造；光束矫形；磁场；热场；超声场

中图分类号 TH164 **文献标志码** A **DOI**：10.3788/CJL231588

1 引 言

激光增材制造（LAM）技术以聚焦后的高能激光束作为热源，根据预先设定的计算机辅助设计（CAD）模型，通过计算机辅助控制逐层熔化原材料，实现成形样品形-性协同控制[1-3]。目前激光增材制造技术中普遍使用高斯激光，聚焦光斑小且中心峰值能量高，使其在高熔点、难加工金属材料的成形上具有独特的优势，可实现复杂金属构件的一体化成形，避免了传统加工工艺繁琐的后处理工序，成形效率高[4]。而且，由于激光与成形材料作用时间短，熔池中熔体的快熔速冷会产生极其精细的微观结构，再加上内部高密度位错，使其制备样品的力学性能接近甚至优于传统铸造或锻造试件，在航空航天、汽车、医疗等领域广受青睐[5-7]。基于激光与粉末的金属增材制造工艺主要包括选区激光熔化（SLM）和激光定向能量沉积（LDED）两种。SLM又称激光粉末床熔融（LPBF），采用辊轮预先铺设粉末，成形面上聚焦光斑较细（80～100 μm），成形精度高，在加工复杂晶格结构、功能超材料、定制骨植入物等方面优势显著[8-15]。LDED又称激光熔化沉积（LMD），采用随激光移动的特制喷嘴同步送粉，成形聚焦光斑相对SLM大（0.5～3 mm），成形精度低，但沉积率比SLM高得多，适用于大尺寸复杂构件的制造或修复[16]。另外，LDED技术粉末进给灵活性高，适用于多材料梯度样品的制备。LAM已广泛应用于多种金属材料的成形，常见的包括铝合金[17]、钛合金[18]、铜合金[19-20]、镍基高温合金[21-22]、镁合金[23]和钢[24-25]等。

高斯激光聚焦光斑中心的峰值能量与边缘的差别巨大，与金属粉末作用时熔池宽深比小且具有较大的温度梯度和冷却速率，复杂的熔体流动动力学所产生的不稳定性以及反复加热和冷却循环的累积效应，极易产生气孔、飞溅、球化、裂纹等冶金缺陷和各向异性的微观组织，严重影响成形部件的强度、韧性以及抗疲劳性能[26-30]。针对上述问题，国内外学者已从不同的角度进行了相关研究。从材料角度来说，进行合金成分改性或添加强化相颗粒可有效改善LAM成形金属样品中的裂纹和各向异性的粗大柱状晶组织，例如：Li等[31]利用SLM原位合金化成形了Ti改性$CoCrFeNiTi_{0.3}$共晶高熵合金，发现熔池边界Ti元素的富集促进成分过冷，使形核率提高并诱导柱状晶向细小等轴晶转变，同时沿晶界析出大量Ni_3Ti纳米沉淀相，合金拉伸屈服强度提高了50%以上；Guo等[32]利用SLM工艺通过原位添加纳米Y_2O_3颗粒抑制了IN738LC高温合金中Zr元素晶界偏析，有效缓解了裂纹的产生。然而，成分改性可能会造成点蚀，降低合金的耐腐蚀性能，且强化相颗粒的添加可能导致颗粒团聚、强化相与基体界面结合差等问题，效果适得其反[33]。从工艺角度来说，热处理是一种消除LAM已成形样品中存在的裂纹等冶金缺陷的有效方法[34-37]。例如Sun等[38]利用热等静压和固溶两步热处理消除了SLM制备GH3536中的微裂纹，使合金拉伸强度和延伸率得到显著提升。但热处理在激光制备的基础上进

收稿日期：2023-12-27；**修回日期**：2024-03-04；**录用日期**：2024-04-02；**网络首发日期**：2024-04-10

基金项目：国家重点研发计划（2018YFB1105301）、中央高校基本科研业务费专项资金（YCJJ20230359）、国家自然科学基金（52275333，51775207，51701078，51905193，52201040）、中国航空制造技术研究院稳定支持项目（KZ571801）

通信作者：*wqs_xn@hust.edu.cn

一步延长了成形时间，增加了工艺的复杂性。

激光矫形和外场辅助可在成形过程中原位调控熔池形态和冷却凝固过程，有望克服LAM中产生的影响成形部件质量的缺陷问题[39]。激光矫形利用非球面透镜组、空间光调制器、衍射光学元件等改变激光束的振幅、相位或传播路径，将高斯激光矫形为不同形状和能量分布形式的激光束。目前已应用于LAM中的矫形激光包括平顶光、反高斯光、贝塞尔光和椭圆形光束[40-42]：平顶激光能量在横截面上均匀分布，反高斯激光能量分布中间低边缘高，贝塞尔激光能量呈现围绕中心的多环形分布，椭圆形激光能量分布呈椭圆形，这4种激光与粉末作用过程中的冶金机理不同。LAM中应用的辅助外场主要有热场、磁场和超声场。热场是通过电阻丝接触基体加热或电磁感应加热等对成形金属进行原位热处理，改变熔池中的温度梯度和冷却速率，达到降低残余应力和抑制裂纹的目的[43-45]；磁场通过洛伦兹力和热电磁对流改变熔池中熔体的流动，从而影响成形金属的晶体取向和相组成等[46-47]；超声场是利用高频声波振动，诱导熔池中产生声流和空化效应，进而影响晶体生长和微观组织[48]。近年来，光束矫形和外场辅助已在不同金属材料的LAM成形中得到研究，包括镍基高温合金、铝合金、钛合金和钢等[49-54]。

本文根据国内外学者和本课题组的研究工作，阐述光束矫形（平顶激光、反高斯激光、贝塞尔激光、椭圆形激光和离焦激光）和热场（电阻丝接触基底预热、电磁感应加热和激光同步预热）、磁场（静态磁场和交变磁场）、超声（超声振动和超声冲击）辅助在SLM和LDED两种金属LAM中的研究进展，揭示不同能量分布形式的光束和热/磁/声场对材料、组织和性能的原位作用机理和影响规律，并对金属激光增材制造技术的未来发展进行展望，以期推动其在多领域的广泛应用。

2 矫形激光增材制造技术

激光能量分布会影响熔池的空间形态，进而影响热梯度和金属冷却凝固过程。目前LAM中普遍使用的是高斯激光，光斑中心峰值能量显著高于边缘区域，导致加工过程中能量利用率较低。高斯激光矫形技术于1965年提出[55]，后被广泛应用于激光焊接、激光切割、激光打标、激光钻孔、激光烧蚀等工艺中。近年来，随着LAM的不断发展，国内外学者探索将矫形激光与金属增材制造技术相结合，以克服高斯激光成形过程中产生的冶金缺陷问题。除了利用光学器件或调制系统将高斯激光矫形为平顶激光、反高斯激光、贝塞尔激光、椭圆形激光外，一些研究还通过调整成形面与焦点之间的距离来改变光斑能量分布，进而达到调控熔池及组织形态的目的。

2.1 平顶激光增材制造技术

平顶激光的能量在横截面上均匀分布，光斑形状包括圆形、矩形等，是最常见的一种矫形激光，在很多领域具有广阔的应用前景。由于SLM和LDED各自具有独特的工艺特征，激光矫形后会产生不同的宏微观冶金规律，因此需对平顶激光在两种工艺中的作用特点进行分别总结和讨论。

SLM工艺中普遍使用的高斯激光成形光斑直径较小（100 μm左右），成形精度高，可实现复杂精细构件的制备，但扫描速率较LDED工艺高1～2个数量级，因此成形过程中具有较大的温度梯度和冷却速率，易产生气孔、飞溅、空隙、高密度位错及杂乱的晶体取向等冶金特征，而平顶激光可实现对SLM成形过程的原位调控。平顶激光光斑能量分布均匀，可有效避免气孔和飞溅产生，例如：Sow等[56]发现平顶光束下熔池稳定，限制了液相蒸发和粉末飞溅，最终成形出近乎致密的IN625样品；Wang等[57]通过数值模拟和单道实验发现平顶激光下熔池温度场较高斯激光更均匀，均匀分布的反冲压力将熔体从中心推向两侧，形成倾斜度较小的匙孔壁，从而降低了反射系数，提高了流场的稳定性。平顶激光下熔池宽深比显著增大，熔池定向散热能力提升，有利于晶体的外延生长，减小局部位错和大角度晶界，例如：Belay等[58]将高斯激光矫形为平顶激光用于制备316L，矫形光路原理图如图1（a）所示，熔池尺寸和宽深比得到显著提高；Huang等[59]使用平顶激光获得了具有较强＜001＞织构的β-Ti柱状晶微观组织，且匙孔效应相较于高斯激光得到有效缓解，高斯激光和平顶激光三维（3D）能量分布如图1（b）所示；本课题组通过实验和数值模拟发现平顶激光下熔池宽深比更大，熔池温度场如图1（b）所示，流场和温度场有利于柱状晶粒的定向外延生长[60]；其他研究也得到了类似结果[61-67]。不仅如此，平顶激光可稳定熔池流场，减少孔隙产生，提高组织致密性，例如：Liu等[68]利用平顶激光成形了AlSi10Mg，激光与粉末作用原理图和熔池形貌光学显微镜（OM）图如图1（c）和图1（d）所示，发现平顶激光下熔池呈传导模式，熔体流动更稳定，飞溅和气孔缺陷减少，样品致密度和表面粗糙度得到显著改善；Okunkova等[69]发现平顶激光下单轨更加规则，冶金结合好且熔池重熔区浅，促进了成形部件几何精度的提高和孔隙率的降低。除此之外，利用平顶激光可实现特殊用途合金的成形，例如Pilz等[70]利用平顶激光制备出沿构建方向显著＜001＞晶体取向的β型Ti-Nb医用合金，该方向上的弹性模量相较于高斯激光成形样品降低了30%以上，有效地避免了应力屏蔽效应，有望实现力学性能匹配骨植入物的个性化定制，熔池扫描电镜（SEM）图如图1（e）所示。

LDED工艺沉积效率高，适用于大尺寸复杂构件的成形，但制备精度和样品表面粗糙度较差。与SLM工艺相比，激光光斑直径较大（0.5～1 mm），而扫描速

率却低得多，成形过程中具有更低的温度梯度和冷却速率，在无外加作用力和形核介质的情况下成形样品晶粒粗大，即使使用高斯激光在一定程度上对晶体的外延定向生长也具有促进作用[71]。国内外学者探索利用平顶激光提高LDED工艺成形样品表面粗糙度，抑制元素偏析和孔隙等缺陷产生，例如：Chen等[72]发现平顶激光可减小LDED制备IN718中的元素偏析，抑制Laves有害相的析出，拉伸屈服强度较高斯激光情况下提升了30%；Wang等[73-74]发现平顶蓝光（450 nm）激光可降低LDED工艺制备AlSi10Mg/TiB_2复合材料中熔池温度梯度，抑制孔隙的产生。另外，平顶激光可提高LDED工艺成形效率，例如Kim等[75]发现方形平顶激光光斑有效能量分布范围较高斯激光大，显著提升了LDED工艺粉末沉积率。与SLM工艺类似，平顶激光可进一步提升LDED成形样品晶体的定向生长，例如：Cheng等[76]利用脉冲平顶激光LDED制备IN718获得了显著的＜001＞方向柱状晶组织，电子背散射衍射（EBSD）图如图1（f）所示；Wang等[77]发现平顶激光中能量的均匀分布可抑制LDED中杂晶和高角度晶界的产生，促进单晶外延生长，成形出低角度晶界比例高于98.5%的无裂纹René N5单晶组织。

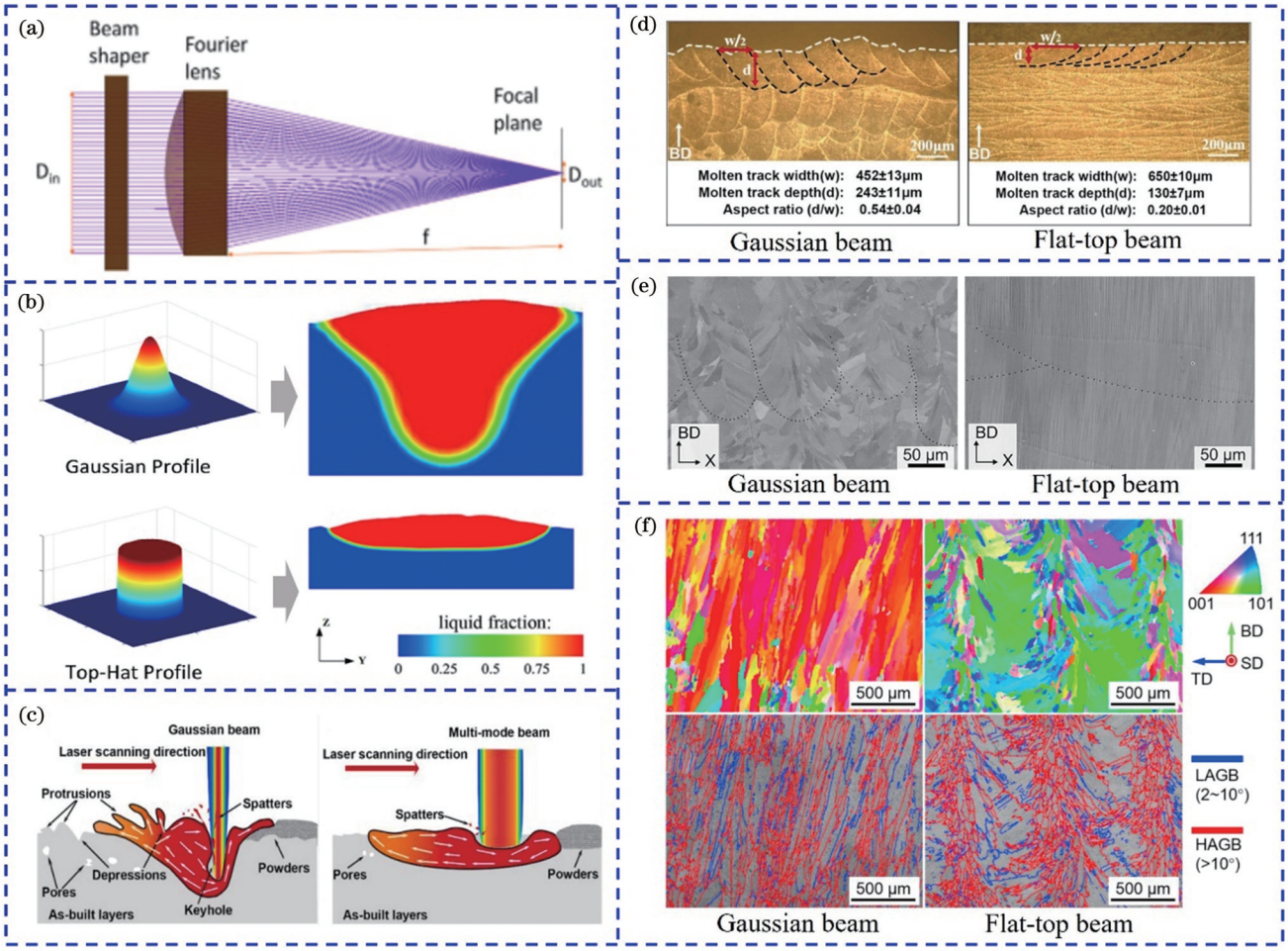

图1 高斯激光与平顶激光增材制造技术对比。（a）光束矫形原理图[58]；（b）能量分布及熔池温度场[59-60]；（c）与粉末作用原理图[68]；（d）AlSi10Mg合金OM图[68]；（e）Ti-Nb合金SEM图[70]；（f）IN718合金EBSD图[76]

Fig. 1 Comparison of Gaussian and flat-top laser additive manufacturing technology. (a) Schematic diagram of beam shaping[58]; (b) energy distribution and temperature field of melt pool[59-60]; (c) schematic diagram of interaction with powder[68]; (d) OM diagram of AlSi10Mg alloy[68]; (e) SEM image of Ti-Nb alloy[70]; (f) EBSD image of IN718 alloy[76]

综上所述，平顶激光由于聚焦光斑能量分布均匀，应用于增材制造技术中可提高匙孔稳定性，改善成形样品表面粗糙度，减少熔体蒸发、粉末飞溅和孔隙产生，提高熔池温度场/流场稳定性和组织致密度，而且熔池宽深比的提高有利于晶粒沿建造方向外延生长，产生显著＜001＞织构组织，可实现特定用途合金样品的制备。

2.2 反高斯激光增材制造技术

反高斯激光横截面上能量分布中间低、边缘高，与高斯激光完全相反。已有研究将反高斯激光应用于金属激光增材制造技术中。Cloots等[78]利用衍射光学元件（DOE）将高斯激光矫形为反高斯激光用于SLM制备IN738LC合金，矫形原理图和制备试样微观形貌如图2（a）和图2（b）所示。从图中可以

看出反高斯激光下熔池宽深比更大，晶粒显示出较高斯激光更明显的<001>取向，表明反高斯激光可达到和平顶激光同样的促进柱状晶粒外延生长的作用。反高斯激光环形部分的能量仅为高斯激光中心峰值能量的40%～50%，可减少制备样品中的气孔缺陷，提高致密度。然而，由于峰值能量的降低，需要提高反高斯激光功率使当前熔融层与已熔融部分实现良好的冶金结合。Wischeropp等[79]利用衍射光学元件M-shaper将高斯激光矫形为反高斯激光用于SLM成形AlSi10Mg合金，单道成形实验表明反高斯激光熔道更平滑，突出和凹陷区域更小，这与反高斯激光下熔池蒸发更少和温度梯度更低有关，抑制了合金中裂纹和气孔等冶金缺陷的产生，使合金致密度得到提升。Grigoriev等[80]通过数值模拟分析了反高斯激光SLM过程中能量分布及熔池温度场，结果如图2(c)所示。从图中可以看出，高斯激光形成的熔池峰值温度出现在中心，逐渐向边缘递减，而反高斯激光熔池中较大区域内温度均匀分布，可有效抑制飞溅和熔体蒸发，CoCr合金单道形貌图表明反高斯激光形成了较高斯激光更宽且更均匀的熔道。因此，反高斯激光下熔池温度分布较高斯激光更均匀，可避免匙孔效应，减少熔体蒸发和飞溅，而且熔池宽深比更大，有利于晶粒的外延生长。

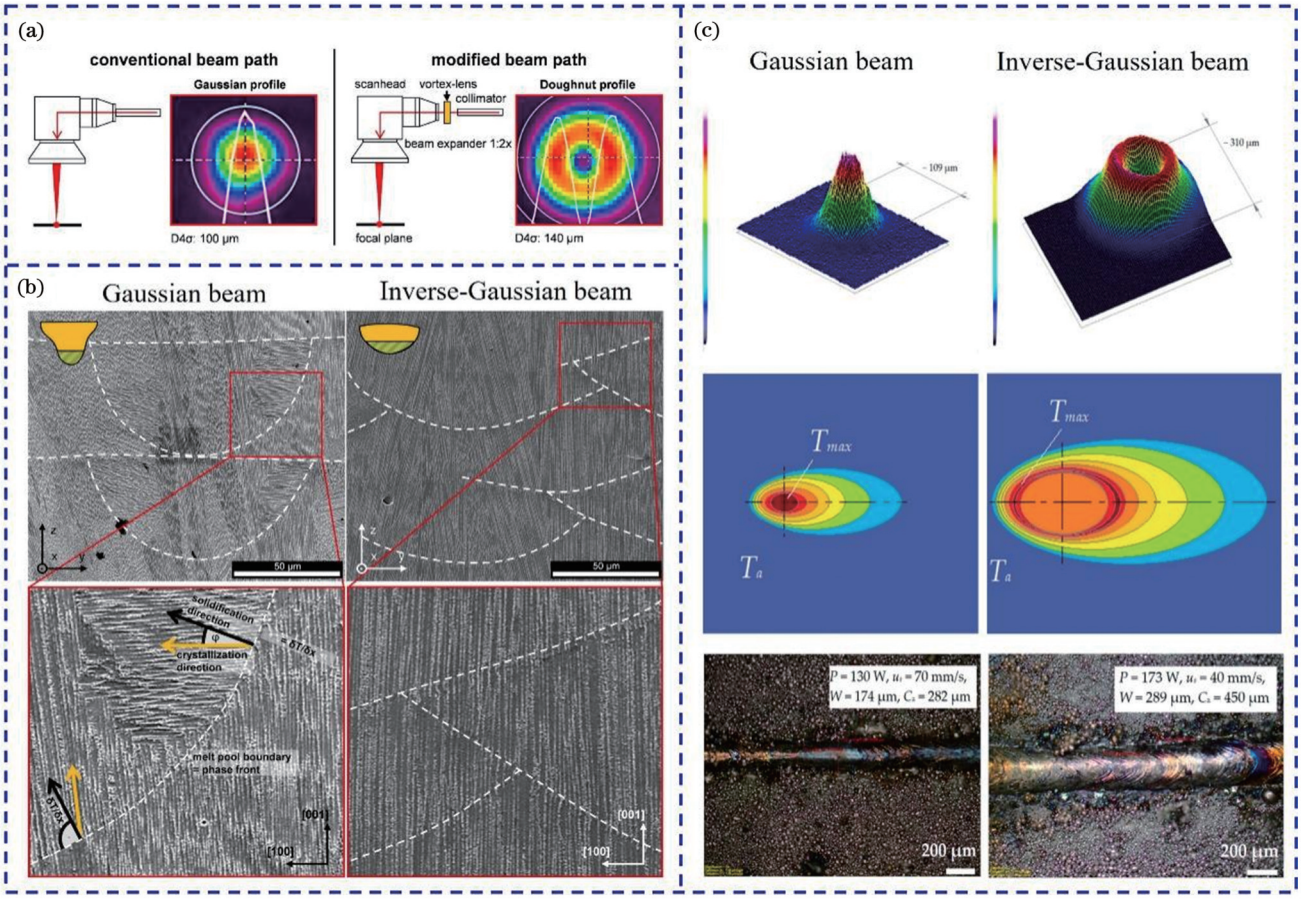

图2 高斯激光与反高斯激光增材制造技术对比。(a)矫形原理及能量分布二维图[78]；(b)制备IN738LC合金SEM图[78]；(c)三维能量分布图、熔池温度平面图及单道形貌[80]

Fig. 2 Comparison of Gaussian and anti-Gaussian laser additive manufacturing technology. (a) Shaping principle and two-dimensional energy distribution diagram[78]; (b) SEM image of IN738LC alloy[78]; (c) three-dimensional energy distribution diagram, temperature distribution of melt pool and single-track morphology[80]

2.3 贝塞尔激光增材制造技术

贝塞尔光束是一种振幅由贝塞尔函数描述的非衍射光束，能量呈现围绕中心能量点的多环形分布，光束中心的能量强度随环数的增加而减小，在测量、校准、医疗、精密加工等方面具有广泛的应用。由于其在传播过程中没有衍射，可以使光束在通过传播路径上的障碍物后自动复原，有利于降低激光增材制造过程中产生的粉末飞溅对激光能量密度的影响[81]。贝塞尔光束可以使用简单的棱镜等光学元件生成，降低了激光矫形工艺的复杂性，尤其对于商用集成3D打印机来说更为友好。而且，由于传统的聚焦光束容易产生强烈的衍射，对在光斑聚焦处准确定位建造平面提出了非常高的要求，而贝塞尔光束在传播过程中无衍射产生，这大大降低了激光增材制造过程中焦平面定位的精度要求，提高了工艺灵活性。上述特点使贝塞尔光束在LAM中具有较大的应用潜力。然而目前

有关贝塞尔激光增材制造技术的研究还较少。Grünewald 等[82]使用环形能量分布的类贝塞尔激光 SLM 制备 316L 合金，由于能量逐渐从中心向边缘转移，降低了聚焦光斑中心与边缘之间的能量梯度，熔池宽深比较高斯激光情况下明显增大，扩大了加工工艺窗口，加工效率得到明显提升。Nahr 等[83]也得到了同样的结果。Tumkur 等[84]使用一对棱镜将高斯激光矫形为贝塞尔光束用于 SLM 制备 316L 合金，矫形原理图及矫形前后能量分布曲线如图 3(a)所示。矫形后激光能量从中心向外围移动，降低了熔体蒸发，改善了熔池中马兰戈尼对流和反冲压力的影响，在相同体积能量密度下贝塞尔激光功率比高斯激光高，获得的熔池深宽比增大但底部更平滑，如图 3(b)所示，在更大的工艺窗口内显著减少了因匙孔熔化模式而产生的气孔缺陷，并且通过高速相机观察到粉末飞溅和熔池湍流得到有效改善，最终获得更加致密、几乎无缺陷的试样。不仅如此，贝塞尔激光还可降低熔池温度梯度，延长其凝固时间，EBSD 结果[图 3(c)]显示晶粒的平均尺寸减小了 30%。因此，贝塞尔激光应用于增材制造工艺中可改善熔体蒸发，抑制熔池对流和飞溅，降低熔池中温度梯度，从而有利于减少气孔等缺陷的产生，提高组织致密性，然而贝塞尔激光与其

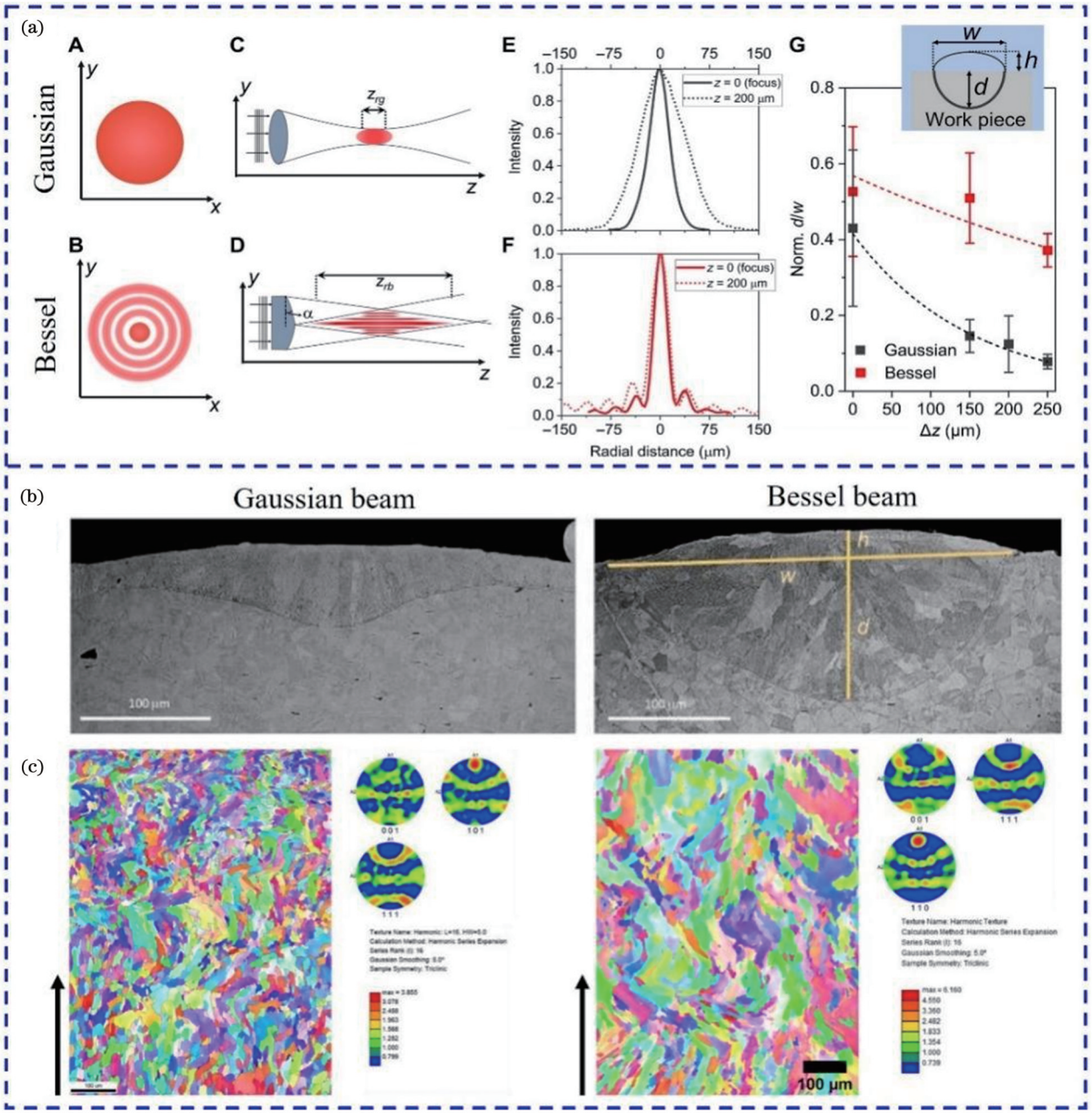

图 3　高斯激光与贝塞尔激光增材制造技术对比。(a)矫形原理图、能量分布及熔池深宽比；(b)形成熔池形貌图；(c)制备 316L 合金 EBSD 图[84]

Fig. 3　Comparison of Gaussian and Bessel laser additive manufacturing technology. (a) Schematic diagram of beam shaping, energy distribution and depth-to-width ratio of melt pool; (b) morphology of formed melt pool; (c) EBSD image of prepared 316L alloy[84]

他材料的作用机理及对微观结构和力学性能的影响还有待进一步研究。

2.4 椭圆形激光增材制造技术

椭圆形激光的空间能量分布同高斯激光类似，但光束横截面呈椭圆形，具有比高斯激光更宽的功率强度范围。有关椭圆形激光增材制造技术的研究相对有限。Roehling等[85]对圆形高斯激光和椭圆形激光分别进行了316L不锈钢SLM单道成形实验和多物理场模拟，激光能量分布如图4(a)所示，由于椭圆光束不同方向上的能量范围宽度不同，对熔池形态和凝固微观结构的影响不同，因此对椭圆形光束主轴平行和垂直于扫描方向分别进行了研究，用LE(longitudinal elliptical)和TE(transverse elliptical)表示。熔融轨道*X*-*Y*、*X*-*Z*、*Y*-*Z*方向的模拟结果如图4(b)所示，LE和TE模式下熔体流速明显高于高斯激光，流速提高将会导致枝晶破碎形成更多形核点，促进等轴化转变。相同光束尺寸和功率下高斯激光和椭圆形激光形成熔道剖面晶粒分布如图4(c)所示，等轴晶粒百分比分别为2%(高斯激光)、28%(LE)和77%(TE)，表明与高斯激光相比，LE和TE模式可显著提高等轴晶区，TE模式最优。另外，使用椭圆形光束可提高熔道的连续性和与基底界面的附着力。随后，该团队在以上研究基础上利用TE模式成形了316L合金块体[86]，结果表明等轴晶粒占的体积分数较高斯激光显著增加，晶粒平均尺寸减小了近50%，晶粒取向结果如图4(d)所示。通过降低激光扫描速度，可以同时实现组织致密化和晶粒细化。基于流体动力学有限元模拟证实等轴晶粒数量的增加与TE模式下较低的热梯度有关。Shi等[87]利用基于流体动力学和元胞自动机晶粒生长算法的有限元模拟进一步揭示了椭圆形激光下等轴化转变的机理。在相同的工艺参数下，TE模式下产生的熔池较高斯激光更浅且更宽，其底部曲率较大，近乎水平；LE模式下熔池较深且窄；高斯激光下熔池形态处于TE和LE之间，如图4(b)中*Y*-*Z*剖面。熔池形态的改变有效降低了温度梯度，使得TE模式下具有最宽的成分过冷区和大的形核倾向，可在更大的工艺窗口内生成等轴晶，实现晶粒细化和力学性能的提高。因此，椭圆形激光相比于高斯激光来说可加快熔池熔体流动，在TE模式下更有利于促进等轴晶形成。然而现有研究仅针对316L等部分材料。未来需要进一步

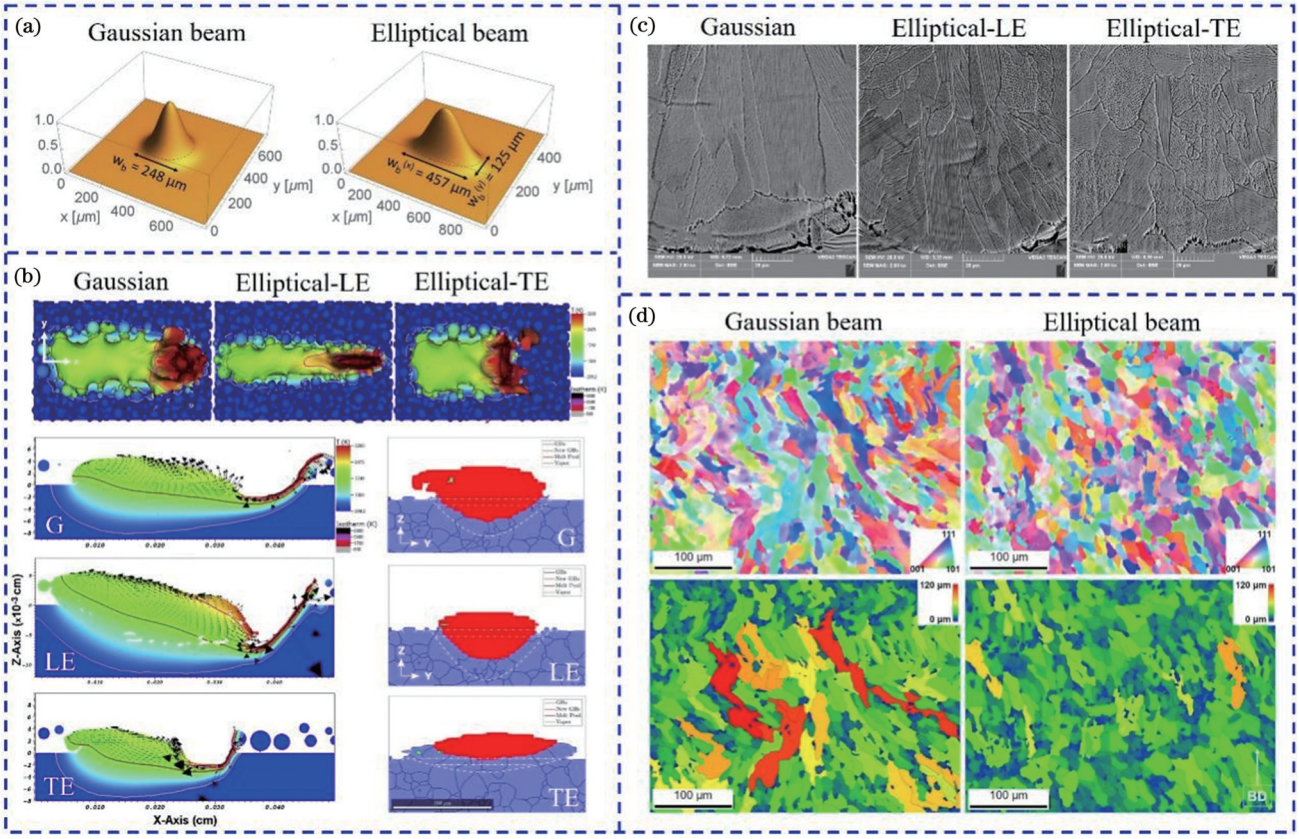

图4 高斯激光与椭圆形激光增材制造技术对比。(a)光斑能量分布图[85]；(b)熔融轨迹热力学模拟*X*-*Y*、*X*-*Z*和*Y*-*Z*面观察(椭圆形光束主轴平行和垂直于扫描方向分别用LE和TE表示)[85,87]；(c) 316L合金熔池底部SEM图[85]；(d) 316L合金侧面EBSD图[86]

Fig. 4 Comparison of Gaussian and elliptical laser additive manufacturing technology. (a) Spot energy distribution diagram[85]; (b) thermodynamic simulation of melt track *X*-*Y*, *X*-*Z* and *Y*-*Z* plane observations (modes with principal axis of elliptical beam parallel and perpendicular to scanning direction are denoted by LE and TE, respectively)[85,87]; (c) SEM image at melt pool bottom of 316L alloy[85]; (d) EBSD image of side of 316L alloy[86]

探究椭圆形激光对其他金属材料微观特征及性能的作用规律。

2.5 离焦激光增材制造技术

离焦光束是通过调节建造平面距离焦点的位置来实现的，可改变成形光斑中的能量密度分布，抑制传统高斯激光因中心峰值能量过高而造成的熔体蒸发、飞溅及气孔等缺陷产生。通常焦点向上偏移为正离焦，向下移动为负离焦。近年来，国内外学者开始将离焦光束应用于金属激光增材制造技术中。

在SLM技术方面，随着离焦量的增加，激光光斑中心与边缘的能量梯度逐渐减小，能量分布趋于均匀化，有利于增大熔池宽深比。根据激光与粉末作用时熔池宽深比的大小，从小到大依次将熔化模式分为匙孔模式、过渡模式和传导模式，匙孔模式下熔池窄而深容易产生气孔等缺陷，而传导模式熔池温度场和流场相对较稳定，有利于减少气孔等缺陷产生，促进晶粒的外延生长，例如：Zhong等[88]研究了激光离焦量对IN718的晶粒生长、微观形貌及力学性能的影响，离焦激光实现原理如图5(a)所示，图5(b)显示了0、5、10、15、20 mm正离焦激光下制备试样侧面形貌，发现随着离焦量的增加，熔池宽深比增大，合金中一次枝晶臂间距减小，等效晶粒尺寸显著增加；Nie等[89]发现由于离焦激光光斑大、能量分布均匀，熔池宽深比大且流场稳定呈传导模式，温度梯度和冷却速率较低，抑制了缺陷形成和裂纹扩展，相较于正焦激光制备样品显微硬度提高了13%；Soylemez[90]通过改变离焦量并建立归一化焓方程得出不产生孔洞缺陷的临界熔池深宽比为0.85；Patel等[91]发现离焦光斑能量分布梯度小，熔池呈传导模式，显著降低了气孔等缺陷的产生，制备出近乎完全致密试样，如图5(c)所示，同时，通过大量工艺参数验证和温度预测模型，总结出传导模式和匙孔模式熔池临界深宽比为0.4；McLouth等[92]发现离焦3 mm激光显著增大了IN718熔池宽深比，降低了熔池中温度梯度和冷却速率，有利于柱状晶粒垂直于熔池底部向上生长，产生显著<001>织构，正焦和离焦激光下晶粒取向如图5(d)所示。除此之外，离焦激光还可改善成形样品表面粗糙度，例如Bean等[93]得出离焦激光使IN718的表面粗糙度降低了28%。

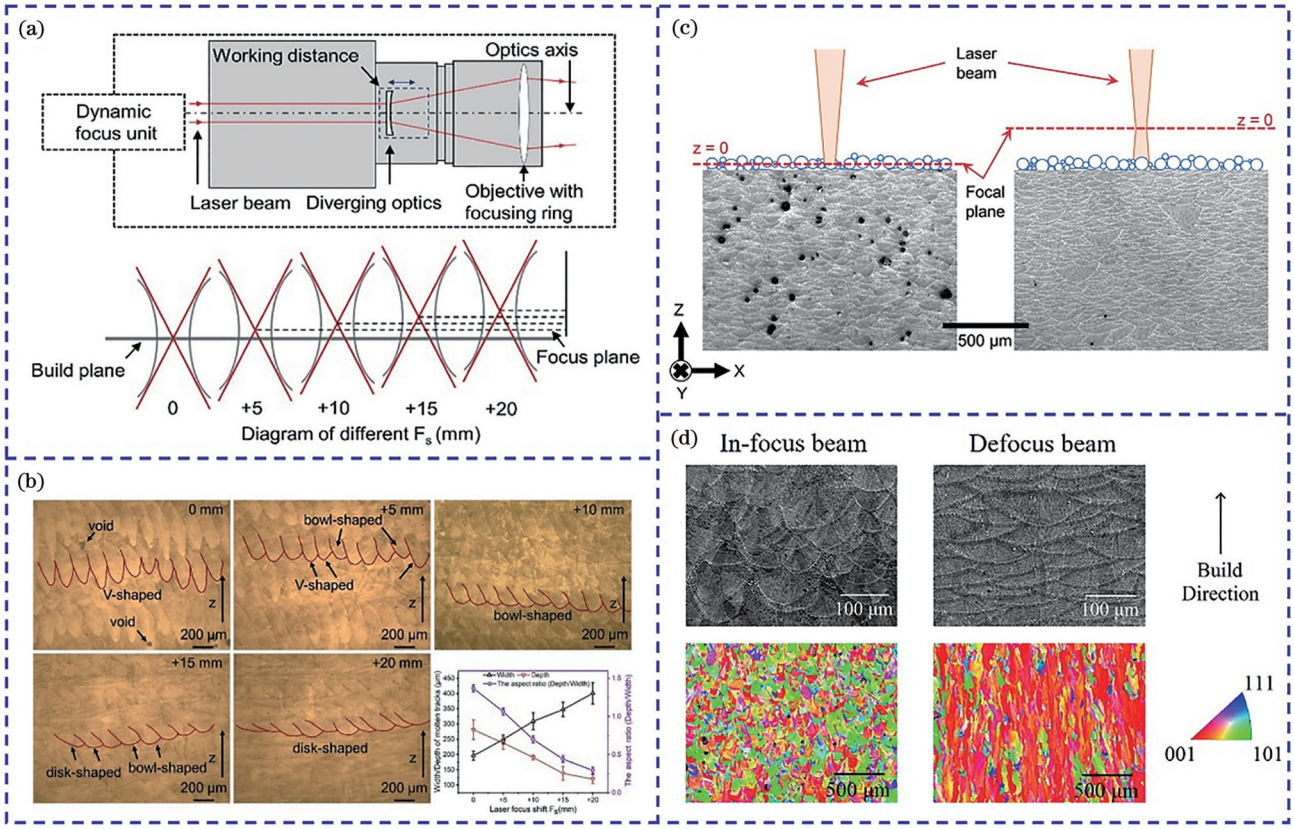

图5 正焦激光与离焦激光增材制造技术对比。(a)离焦激光实现原理图[88]；(b)离焦量分别为0、5、10、15、20 mm时IN718合金侧面OM图[88]；(c) AlSi10Mg合金侧面OM图[91]；(d) IN718合金侧面SEM和EBSD图[92]

Fig. 5 Comparison of additive manufacturing technology between focusing laser and defocusing laser. (a) Schematic diagram of defocusing laser[88]; (b) OM diagrams of IN718 alloy with defocus of 0, 5, 10, 15 and 20 mm, respectively[88]; (c) OM diagram of AlSi10Mg alloy [91]; (d) SEM and EBSD images of side of IN718 alloy[92]

由于LDED与SLM工艺上存在差异，离焦激光应用于LDED中可能会产生与SLM不同的冶金效果，例如Zhao等[94]在LDED制备镍基高温合金过程中，通过改变离焦量获得能量分布均匀的激光束，使熔池温度

梯度降低，增加成分过冷，样品的微观结构从柱状晶变成了密集排列的等轴晶。然而离焦激光应用于LDED相关研究相对有限，未来需要进一步探索离焦激光在LDED工艺中的冶金机理和工程应用价值。

离焦激光实现成本低，工艺简单，并可获得与平顶激光类似的促进晶粒外延生长、减少气孔等缺陷和改善样品表面粗糙度的效果，未来在金属激光增材制造技术中具有较大的应用潜力。

综上所述，高斯激光由于能量从光束中心向边缘的径向变化在熔池中产生较大的热梯度，造成制备样品中极易出现孔隙、裂纹等缺陷。矫形后的平顶激光能量均匀分布；反高斯激光能量呈中间低边缘高的环形分布；贝塞尔激光能量呈多环形分布；离焦激光的离焦量越大，光斑越大，能量分布相对于焦点激光越分散。四种矫形激光均在不同程度上使传统高斯激光中心峰值能量减弱，降低了熔池中的温度梯度，抑制了粉末蒸发和飞溅产生，提高匙孔稳定性，从而可在更宽的工艺窗口内减少气孔、裂纹等缺陷的数量，获得近乎致密的样品。从对晶粒取向的影响来看，平顶激光、反高斯激光和离焦激光形成的熔池宽深比增大，可促进柱状晶外延生长，尤其是平顶激光能量分布均匀，可获得近乎完全<001>取向的织构，这对于制备单晶、β型医用钛合金等优势显著。相比之下，椭圆形光束轮廓对凝固微观结构有很大影响，通过降低熔池温度梯度、增大成分过冷区来提高形核倾向，促进等轴晶生成，实现晶粒细化和组织致密化，表明通过改变光束强度剖面形状可定制晶粒形态。随着激光矫形技术的不断成熟，未来将进一步拓展金属激光增材制造技术在各领域的广泛应用。

3 热场辅助激光增材制造技术

激光增材制造是一个高度瞬态的过程，金属熔体在激光束作用下经历了反复加热和冷却的循环过程，且高斯激光中心过高的峰值能量使熔池中存在较大的热梯度，导致成形部件内部残余应力及裂纹产生。在激光增材制造过程中进行外部热量输入本质上是一种原位热处理的过程，可有效降低熔池中的温度梯度，调控金属熔体的冷却和凝固过程，从而达到抑制缺陷的目的[95]。常见的金属激光增材制造技术辅助热场包括电阻丝接触基底预热、电磁感应加热和激光同步预热。

3.1 电阻丝接触基底预热

基底预热的热量由成形缸底部的热电阻丝产生，自下向上通过接触传导到成形表面，可对熔池温度梯度进行调控，是一种普遍使用的缓解残余应力和裂纹的方法，例如：Lu等[96]通过热力学分析表明700 ℃预热会使LDED制备Ti6Al4V的残余应力和最终变形分别减少80.2%和90.1%；Polozov等[97]发现900 ℃预热可有效抑制SLM制备Ti48Al2Cr2Nb合金中裂纹产生，致密度达到99.9%，压缩强度优于传统工艺试样，不同预热温度（600、800、900 ℃）下样品形貌如图6(a)所示。基底预热还可通过原位时效作用调控相组成和晶粒生长行为，增强合金力学性能，例如：Gussone等[98]发现800～1000 ℃预热促进SLM成形TiAl合金中γ相大量形成，获得了与传统制备工艺相当的拉伸强度（545 MPa）；Deng等[99]得出700 ℃预热促进SLM成形Ti55531合金β基体中析出α纳米强化相，极限拉伸强度达1440 MPa，硬度达8.24 GPa；Zhu等[100]得到150 ℃预热促进SLM制备AlSi10Mg中原位析出颗粒状或棒状Si相和针状β″相，屈服强度提高了近10%；Nezhadfar等[101]发现150 ℃预热促进SLM制备316L合金中<001>取向大尺寸柱状晶向<011>、<111>精细等轴晶转变，增强了合金延展性和疲劳强度，预热与未预热样品的微观形貌如图6(b)所示；Liang等[102]发现180 ℃预热促进SLM成形ZK60中析出大量β_1'强化相，显著增强了镁合金力学性能，然而β_1'析出相与α-Mg基体形成大量微电偶池，同时也降低了合金耐腐蚀性能；Chen等[103]发现700 ℃预热使SLM制备IN738LC合金中高角度晶界减少，抑制了热裂纹的产生和扩展，晶界MC碳化物和细小γ′强化相随预热温度升高大量析出，极限拉伸强度（≈1612 MPa）和延伸率（≈18%）显著增强。

基底预热会造成沿建造高度温度分布不均，从而使金属产生梯度分布的不均匀微观组织。Chambrin等[104]发现170 ℃预热造成SLM成形AlSi10Mg合金沿成形高度方向各向异性的力学性能，样品中接近基板的部分产生了过度时效，断裂能最高，硬度最低，峰值硬度出现在距离基板40 mm高的位置。Karjňák等[105]发现500 ℃预热促进SLM制备Ti-8.5Mo合金中β相向α相转变，抑制了ω相形成，使合金沿建造高度方向产生了不均匀的相分布，顶层主要为β+ω相，底部主要为β+α相，从而造成了顶部硬度高、底部硬度低的各向异性的力学性能。Cui等[106]发现500 ℃预热导致SLM成形FeCoMo合金中原位析出μ相的含量沿高度方向出现明显差异，近基板位置层间温度$T_N>M_s$（T_N为成形样品层间温度；M_s为马氏体转变起始温度），μ相未在奥氏体中析出，可减少裂纹的产生，随着距离基板高度增加，中间层$T_N<M_s$以及近顶层$T_N<M_f$（M_f为马氏体转变终止温度），μ相在逐渐增多的马氏体中析出，易产生裂纹，成形样品温度分布如图6(c)所示。

预热温度过高会对材料微观组织及性能带来不利影响，例如：Ali等[107]在SLM制备Ti6Al4V中将粉末床温度提高到570 ℃，可显著减少部件内残余应力，这一预热温度使α'马氏体相分解为α+β平衡相组织，从而合金屈服强度和伸长率分别提高了3.2%和66.2%，但是继续提高预热温度（770 ℃）会导致屈服强度和延伸率急剧下降，这主要与α相球化和晶界β相长大有关；Baek等[108]在LDED制备M4工具钢过程中采用

200～300 ℃预热，可有效降低残余应力，抑制裂纹产生，由于共晶碳化物析出和晶粒长大，硬度增大而强度和韧性略有下降，但预热温度继续增加至 500 ℃时会导致晶粒及晶界碳化物严重粗化，试样强度和韧性急剧下降；Zhou 等[109]发现 200 ℃预热抑制 SLM 制备 Ti-15Mo 中纳米级强化相 ω 相析出，而且使晶粒粗化，减小了合金中位错密度，与未预热条件下制备试样相比极限拉伸强度和硬度显著降低。预热温度对组织和性能的影响与成形材料内相转变温度密切相关，例如 Mertens 等[110]发现 400 ℃预热显著减少 Al7075 裂纹产生，使其微观结构更加均匀，并且促进 H13 工具钢硬度和极限拉伸强度的提升，这是由于 Al7075 中脆性相 $MgZn_2$ 的析出和 H13 工具钢中的奥氏体-马氏体转变都发生在 400 ℃以下，400 ℃预热会抑制 $MgZn_2$ 相析出，使 H13 合金钢中保持奥氏体组织，冷却至室温后形成硬度更高的贝氏体组织。然而，基底预热对于难加工金属材料来说仍存在挑战，如 Müller 等[111]研究发现 1000 ℃预热仍无法完全抑制 SLM 制备纯钨样品中微裂纹的产生。

本课题组研究了基板预热温度对 SLM 制备 Ti45Al2Cr5Nb 合金织构、相及纳米硬度的影响[112]，结果表明预热温度的提高降低了冷却速率，导致晶粒粗化，不同预热温度（25、150、250、350 ℃）下 EBSD 结果如图 6(d)所示。由于预热导致 α_2 相降低，γ 和 B_2 相增多，从而提高了合金的纳米硬度，不同预热温度下合金加载/卸载曲线和纳米硬度值如图 6(e)所示。综上所述，基底预热降低了成形过程中熔池温度梯度，减少了热应力，可有效抑制裂纹产生，然而预热温度过高可能会对材料组织和性能产生不利影响，应根据成形材料相转变温度设定合理的预热温度。

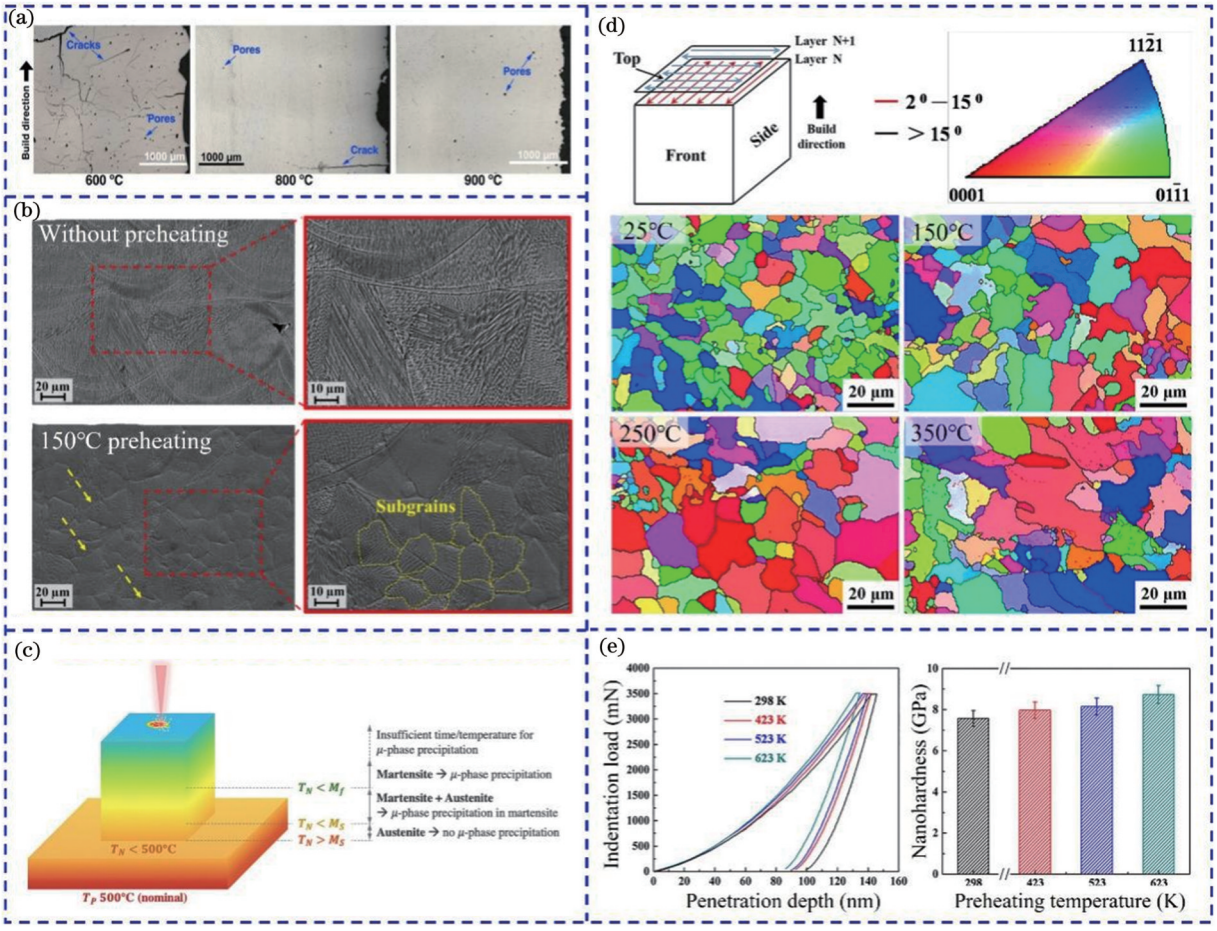

图 6 基底预热辅助激光增材制造技术。(a) 600、800、900 ℃预热下 TiAl 合金 OM 图[97]；(b)未预热和 150 ℃预热下 316L 显微形貌图[101]；(c) 500 ℃预热下成形 FeCoMo 合金温度分布[106]；(d) 25、150、250、350 ℃预热温度下 TiAl 合金 EBSD 图[112]；(e)不同预热温度下 TiAl 合金加载-卸载曲线和纳米硬度值[112]

Fig. 6 Substrate preheating assisted laser additive manufacturing technology. (a) OM diagrams of TiAl alloy preheating at 600, 800, 900 ℃[97]; (b) 316L microstructure without preheating and with preheating at 150 ℃[101]; (c) temperature distribution of FeCoMo alloy fabricated at 500 ℃ preheating[106]; (d) EBSD images of TiAl alloy at preheating temperature of 25, 150, 250, 350 ℃[112]; (e) loading-unloading curves and nano-hardness values of TiAl alloy at different preheating temperatures[112]

3.2 电磁感应加热

电磁感应加热的热场是通过电磁感应使放置在线圈中的金属内部产生涡流而产生的，可对激光增材制造成形构件整体进行均匀预热，通常能达到较

基底预热更高的预热温度，实现对成形构件内部组织和性能的调控。Shim 等[113]利用感应加热辅助 LDED 制备 M4 工具钢过程中发现 500～700 ℃预热可促进脆性马氏体分解，提高试样拉伸强度，降低裂纹敏感性，尽管预热会导致晶粒粗化，但更高体积分数碳化物的析出会使合金硬度增加。Caprio 等[114]设计了一套感应加热系统，如图 7(a)所示，可将 SLM 制备 γ-TiAl 合金过程中粉床和基板预热至 800 ℃，有效抑制了裂纹，改善了合金脆性，致密度可达 99% 以上，预热和未预热样品显微形貌如图 7(b)所示。Dalaee 等[115]在 LDED 制备 IN625 过程中采用电磁感应预热显著提高了粉末沉积速率和加工效率，电磁感应加热原理如图 7(c)所示。Fan 等[116]利用有限元模拟表明同步感应加热辅助激光定向能量沉积过程中的热应力大幅降低(约 80%)，最大应力的位置从沉积的底角移到了基底的中间区域。电磁感应加热辅助 LAM 过程中熔池内受到热场和感应磁场共同作用，可能会产生未被发现的复杂冶金过程，因此，还需要对电磁感应加热辅助 LAM 技术进行深入研究。

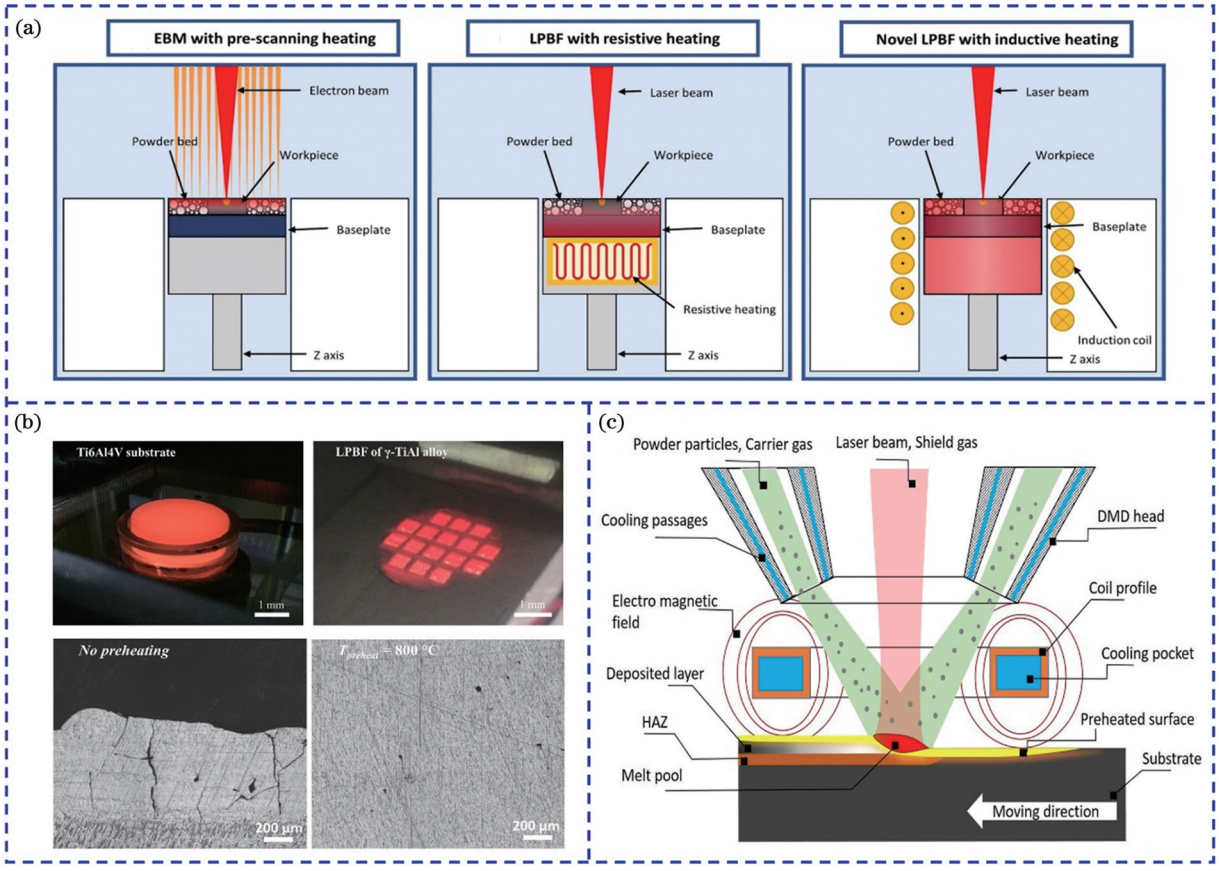

图 7　电磁感应加热辅助激光增材制造技术。(a)激光同步预热、电阻丝基底预热和电磁感应加热原理图对比[114]；(b)电磁感应加热过程照片及无预热和 800 ℃预热下 TiAl 合金显微形貌[114]；(c)电磁感应辅助 LDED 原理图[115]

Fig. 7　Electromagnetic induction heating assisted laser additive manufacturing technology. (a) Comparison of schematic diagram of laser scanning preheating, resistance wire preheating and electromagnetic induction heating[114]; (b) photos of electromagnetic induction heating process and microstructure of TiAl alloy without preheating and with preheating at 800 ℃[114]; (c) schematic diagram of electromagnetic induction-assisted LDED[115]

3.3　激光同步预热

激光同步预热是利用低功率激光扫描成形区域，可对成形层进行选择性实时预热，可减少对周围未使用粉末预热而造成的能量损失，提高预热效率[117]。激光同步预热可有效改善成形构件中的残余应力和裂纹问题。Yan 等[118]通过有限元模拟验证了利用能量分布均匀的超高斯光束用于预热，高斯光束用于熔化，反高斯光束用于后热处理可以显著降低 LDED 制备 Ti6Al4V 中的残余应力。Meng 等[119-121]利用激光同步预热辅助 LDED 成形了无裂纹 316L/IN625/Ti6Al4V 功能梯度材料，裂纹的抑制与铬/钼富集相析出减少和残余应力的降低有关，激光同步预热过程、预热和未预热样品显微形貌、成形试样如图 8(a)～图 8(c)所示。Chen 等[122]通过数值模拟证明了采用第二束激光垂直后加热策略使成形样品中残余应力从 1068.64 MPa 降低至 760.21 MPa。Maurya 等[123]利用激光预热扫描降低了 SLM 制备 TiC-430L 陶瓷基复合材料的残余应力，抑制了裂纹，但无法完全消除气孔缺陷，扫描预热过程如图 8(d)所示，但预热激光扫描速度过低会导致能量密度升

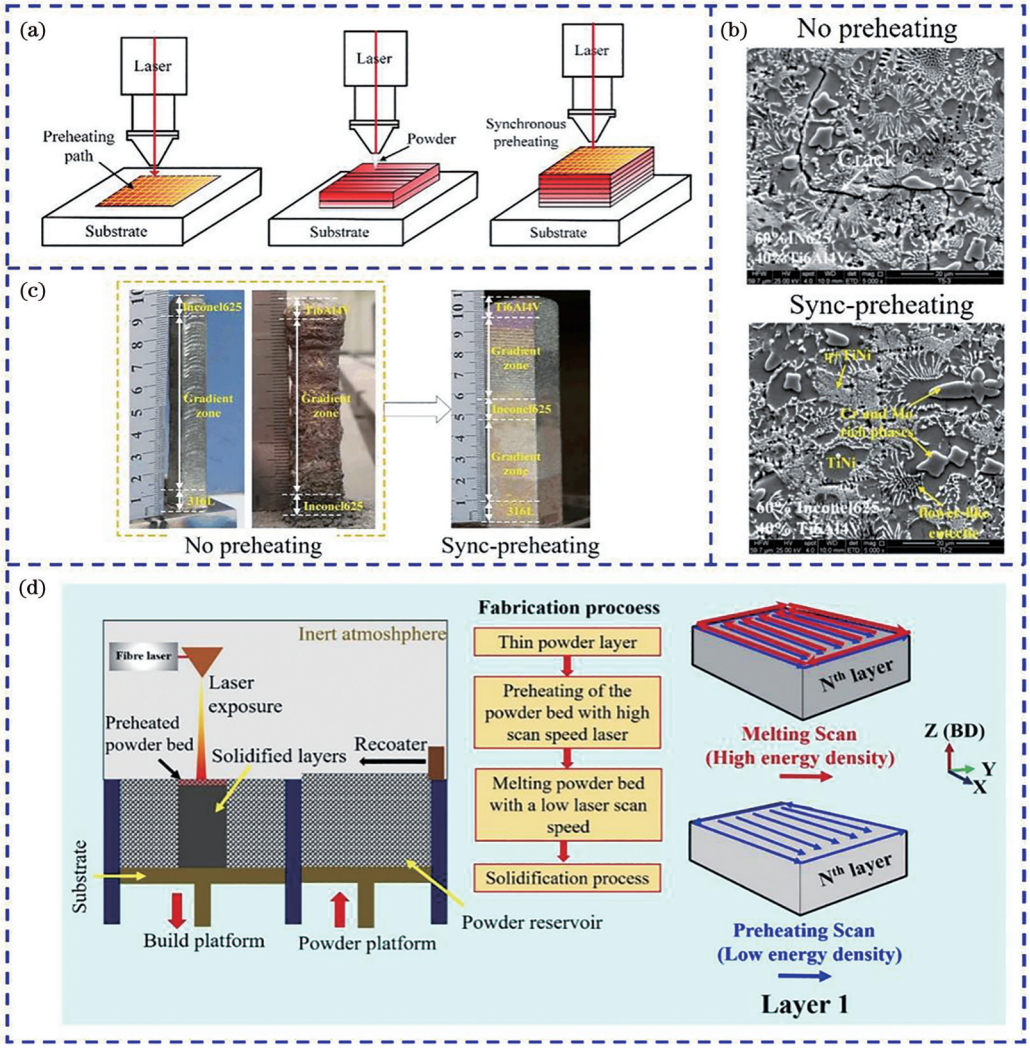

图 8 激光同步预热辅助激光增材制造技术。(a) LDED 过程中激光同步预热过程[121];(b) 60%IN625-40%Ti6Al4V 复合材料预热和未预热显微形貌[120];(c)预热和未预热下制备样品照片[119];(d)激光扫描辅助 SLM 工艺过程示意图[123]

Fig. 8 Laser scanning preheating assisted laser additive manufacturing technology. (a) Laser synchronous preheating in LDED process[121]; (b) microstructure of 60%IN625-40%Ti6Al4V composites with and without preheating[120]; (c) photos of prepared samples with and without preheating[119]; (d) diagram of laser scanning assisted SLM process[123]

高,增加成形部件中的残余应力,因此需合理设置预热激光功率和扫描速度。Zhang 等[124]通过热力学计算得出低功率激光预热使残余应力降低了 10.41%。综上所述,激光同步预热可减少成形层中温度梯度,从而减少样品中的残余应力,达到抑制裂纹产生的效果。

综上所述,基底预热、电磁感应加热和激光同步预热三种方式均可有效降低激光增材制造过程中熔池热梯度,缓解成形部件中的高残余应力和裂纹。对比来看,基底预热形成的热场从下至上通过接触逐渐传导至成形件表面,工艺简单,但会造成成形构件沿高度方向不均匀的微观组织和性能,且受限于激光增材制造设备高度集成性,很难达到高预热温度;电磁感应加热可对成形构件整体进行均匀预热,避免了预热不均而造成的组织各向异性,且可以实现较高温度预热,但工艺复杂,对激光增材制造设备要求较高;激光同步预热可对成形区域进行精确预热,降低了热量损失,热场自上而下进行传导,然而激光预扫描加热的过程延长了制备时间,降低了激光增材制造成形效率。由于成形材料的微观组织和性能会随预热温度而变化,因此需进一步揭示材料-预热工艺参数-激光扫描参数-组织-性能之间的关系。

4 磁场辅助激光增材制造技术

金属冷却凝固过程中,熔体的流动对成形样品的组织及性能有重要的影响。磁场可通过作用于液态金属内部的洛伦兹力来调控熔体的流动,在铸造、焊接等传统工艺中应用广泛,已被证实可用于控制溶质偏析[125]、细化传统铸造中的枝晶臂间距[126]、实现液态锂的自搅拌[127]等。近年来,国内外学者开始探索将磁场应用于金属激光增材制造技术中以克服其面临的工艺缺陷问题,常见的辅助磁场包括静态磁场和交变磁场。

4.1 静态磁场

静态磁场是一种大小和方向不随时间而变化的恒稳磁场，可通过永磁体或通恒定电流的电磁体来产生。激光增材制造过程中形成的熔池会产生较大的热梯度，从而在塞贝克效应的作用下自发地产生热电流，当施加外部磁场时，热电流和磁场的相互作用会形成洛伦兹力，在熔池中形成热电磁对流推动熔体流动。国内外学者针对静态磁场应用于 SLM 和 LDED 成形过程进行了广泛研究。

SLM 工艺方面，静态磁场有助于稳定熔体流动，缓解因匙孔导致的冶金缺陷问题，促进组织致密化，例如：Du 等[128]发现 0.2 T 磁场可减少 AlSi10Mg 和 IN718 中的孔隙缺陷，提高合金致密度并扩大工艺窗口，熔池动力学模拟揭示孔隙缺陷的减少与激光吸收率增加有关；Wang 等[129]模拟得出磁场诱导产生的洛伦兹力使熔池中流场趋于平稳并抑制匙孔波动；Zhou 等[130]发现磁场作用下的磁阻尼效应抑制了 AlSi10Mg 熔体中的马兰戈尼对流，提高了热扩散率和熔池动态运动稳定性，减少飞溅产生并有助于熔体中气体溢出，提高合金致密度。磁场可调控合金冷却凝固过程中的溶质分布和相组成，提升整体力学性能，例如：Kang 等[131]发现磁场促进纯钛中精细针状马氏体 α′-Ti 的析出，样品延展性提高了近 30%；Zhu 等[132]发现 0.1 T 磁场使 IN625 中 Laves 有害相析出量减少了近 50%。磁场诱导产生的热电磁力可诱导枝晶破碎，促进晶粒细化，例如：Du 等[133]发现磁场促进 AlSi10Mg 中柱状晶向等轴晶转变，减小了枝晶臂间距，合金极限拉伸强度和延伸率分别提高近 25% 和 50%，磁场辅助 SLM 工艺原理和热电磁力模型分别如图 9(a)和图 9(b)所示；Nie 等[134]发现 0.55 T 磁场下作用于枝晶上的热电磁力达 10^6 N/m^3，可使生长较快的柱状晶破碎，达到细化晶粒的效果。另外，磁场还会影响晶体生长行为，改变组织织构特

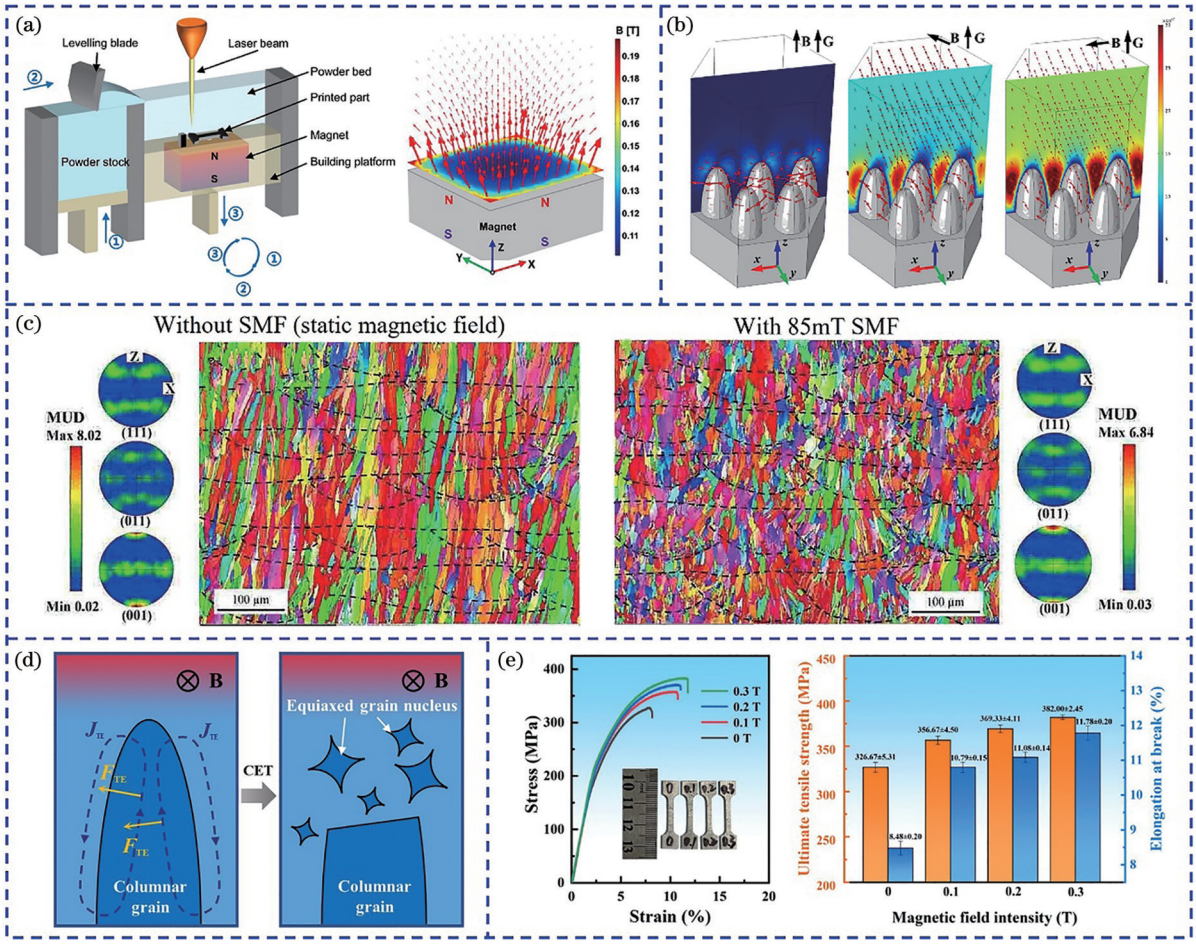

图 9 静态磁场辅助激光增材制造技术。(a)静态磁场辅助 SLM 原理图及场强分布[133]；(b) 0.12 T 静态磁场中作用于枝晶上的热电磁力三维模拟结果[133]；(c)无磁场和 0.85 mT 静态磁场辅助 SLM 制备 AlSi10Mg 合金 EBSD 图[130]；(d)热电磁力诱导枝晶破碎原理图[17]；(e) 0、0.1、0.2、0.3 T 磁场辅助下 SLM 制备 AlSi10Mg 拉伸应力-应变曲线及力学性能[17]

Fig. 9 Static magnetic field assisted laser additive manufacturing technology. (a) Schematic diagram of static magnetic field-assisted SLM and field intensity distribution[133]; (b) 3D simulation results of thermal electromagnetic force acting on dendrites in 0.12 T static magnetic field[133]; (c) EBSD image of AlSi10Mg alloy prepared by SLM with 0.85 mT and without static magnetic field[130]; (d) schematic diagram of thermal electromagnetic force-induced dendrite breakage[17]; (e) tensile stress-strain curves and mechanical properties of AlSi10Mg prepared by SLM with the assistance of 0, 0.1, 0.2 and 0.3 T magnetic fields[17]

征，例如：Zhou 等[130]发现磁场抑制晶体的外延生长，<001>取向减弱，有/无磁场下 EBSD 对比结果如图 9(c)所示；Wang 等[135]也观察到磁场作用下 Al-Si 合金中<001>织构取向的降低；本课题组研究得到 0.1～0.3 T 磁场使 AlSi7Mg 晶体取向由<001>变为<110>和<111>[17]，这主要是热电磁力促使外延生长的枝晶破碎诱导再结晶的结果，如图 9(d)所示，而且随着磁场强度的增加，晶粒尺寸逐渐减小，等轴晶比例增加，合金极限拉伸强度和延伸率显著增强，不同强度磁场下的力学性能如图 9(e)所示。

磁场在 LDED 工艺中的作用与 SLM 类似，可调控熔体流动和溶质分配行为，促进晶粒细化和力学性能的提高，例如：Filimonov 等[136]发现 0.2 T 磁场诱导产生的热电磁对流有效减少了 IN718 富铌有害相的析出，极限伸长率提高了 4%；Chen 等[137]模拟揭示磁场在熔池中产生的洛伦兹力抑制马兰戈尼对流效应，促进熔池熔体流动更加平稳，有利于形成更光滑的成形件表面，另有其他研究也得到相似结果[138-139]；Zhao 等[140]发现 0.55 T 磁场促进 Ti6Al4V 中 β-Ti 柱状晶细化，取向由强<001>纹理逐渐变为弱<110>，不连续 α-Ti 增多，合金延伸率显著提高。磁场不仅会影响 LDED 中熔池冶金过程，还会对粉末产生作用，例如 Smith 等[141-142]在 LDED 过程中施加与激光束同轴的通电螺线管，发现所产生的磁场使送粉更加聚集，粉末利用率提高了 25%。

因此，静态磁场可稳定熔池流动场，减少气孔等冶金缺陷，调控溶质分布行为和合金相组成，更为关键的是，磁场诱导产生的热电磁力可导致枝晶破碎，有效促进晶粒细化和等轴化转变，使合金力学性能得到增强。

4.2 交变磁场

交变磁场可利用通交变电流的电磁体或螺线管产生，其通过洛伦兹力和感应电流共同影响熔池冶金凝固过程。交变磁场辅助激光增材制造技术国内外研究相对有限。Zhou 等[143]研究了轴向静态磁场(20 mT)和交变磁场(0.4 mT，300 Hz)对 SLM 制备 SS316L 合金显微组织和力学性能的影响，工艺原理如图 10(a)所示，结果表明静态磁场和交变磁场均抑制了晶粒外延生长，静态磁场下试样表现出强<110>织构取向，

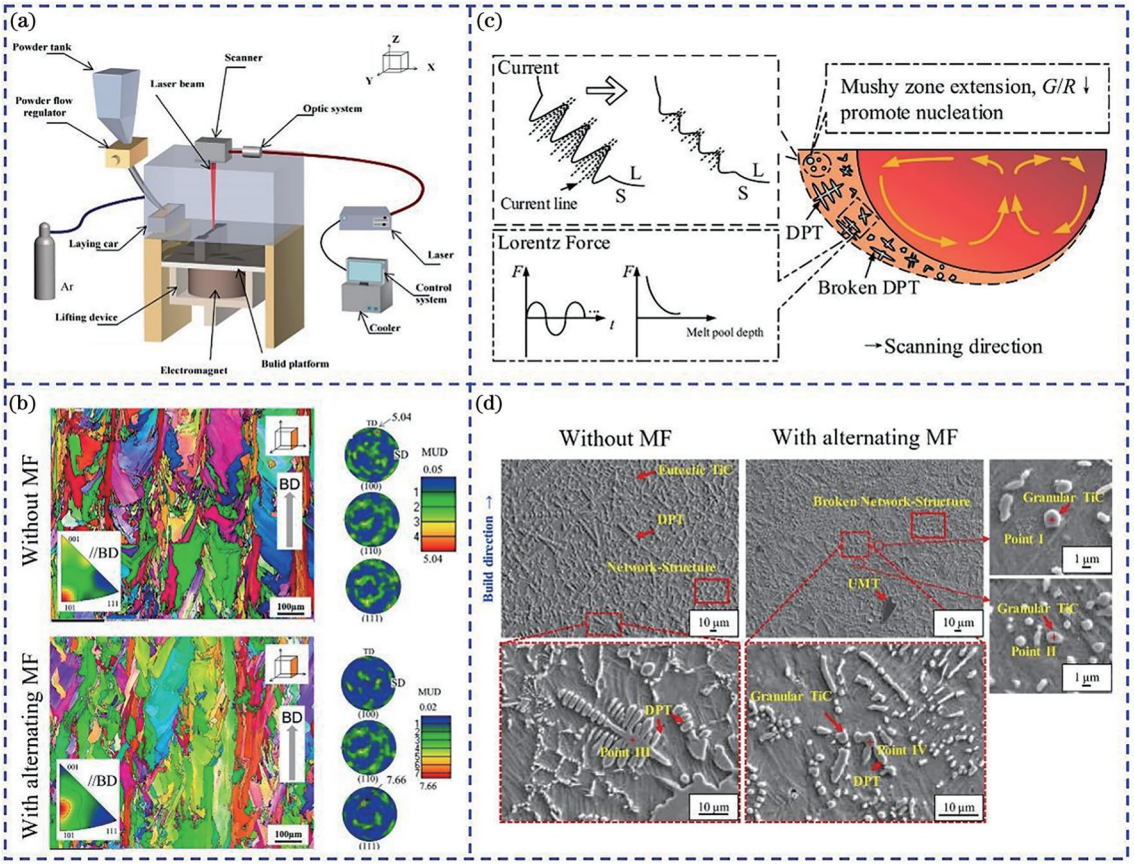

图 10 交变磁场辅助激光增材制造技术。(a)交变磁场辅助 SLM 实现原理图[143]；(b) 0.4 mT，300 Hz 交变磁场与无磁场下制备 316L 合金 EBSD 图[143]；(c)同步电磁感应辅助 LDED 熔池凝固行为[144]；(d)无磁场和高频电磁场下 TiC 增强 Ti6Al4V 合金微观形貌[144]

Fig. 10 Alternating magnetic field assisted laser additive manufacturing technology. (a) Schematic diagram of alternating magnetic field-assisted SLM[143]; (b) EBSD image of 316L alloy prepared under 0.4 mT, 300 Hz alternating magnetic field and no magnetic field[143]; (c) solidification behavior of melt pool in synchronous electromagnetic induction-assisted LDED process[144]; (d) micro-morphology of TiC enhanced Ti6Al4V alloy with and without high-frequency electromagnetic field[144]

延伸率显著提高，达52.6%；交变磁场下感应电流和洛伦兹力的交互作用使熔体对流加强，熔池冷却速率增加，晶粒明显细化，显示出强<102>织构取向，拉伸强度和延伸率得到有效提升，无磁场和交变磁场下制备样品EBSD结果如图10(b)所示。Ma等[144]在LDED制备TiC增强Ti6Al4V过程中施加了750 kHz的高频电磁场，在熔池中产生的不断变化的洛伦兹力促进了枝晶破碎，熔池凝固行为如图10(c)所示，从而促使脆性原生TiC细化且数量减少，无磁场和高频电磁场下制备样品微观形貌如图10(d)所示，制备合金拉伸强度与未施加磁场相比提高了7.5%。Zheng等[145]发现交变磁场诱导的电磁搅拌能有效增强IN718中树枝状晶之间的对流，这不仅有助于形成更细的树枝状晶，还能缓解固液界面元素Nb、Mo的富集，并抑制Laves相的析出。因此，交变磁场下熔体受感应电流和洛伦兹力作用，可加快熔池中对流效应，减少偏析并促进枝晶破碎，起到细化晶粒、提高力学性能的作用。由于交变磁场对熔池中液态金属凝固及晶粒生长作用机理较静态磁场更复杂，因此未来需针对不同成形材料进行深入研究。

综上所述，静态磁场和交变磁场辅助金属激光增材制造技术在成形不同材料时已证实具有优异的效果，通过产生的洛伦兹力和热电磁对流调控熔池中熔体流动，从而细化晶粒，促进各向同性的等轴晶区形成，并抑制有害相析出，实现力学性能的提升。相较于静态磁场，交变磁场对熔池凝固的作用机理更为复杂，除了磁场的作用外，还需考虑由于涡流而产生的热场的影响。未来需进一步研究磁场大小、频率及作用方向对激光增材制造成形不同材料的影响规律。

5 超声辅助激光增材制造技术

超声波是一种波长小于2 cm的依靠介质进行传播的机械波，通过高频振动对位于其形成的超声场中的物体产生作用，在材料制备、加工以及检测方面应用广泛。近年来，为克服LAM中因高温度梯度和往复循环加热、冷却而造成的晶体粗大和复杂残余应力问题，研究者探索将超声场引入LAM成形过程中实现对冶金过程的原位调控，提升制件的综合力学性能。超声波与LAM成形过程的原位作用方式主要包括超声振动和超声冲击强化两种。

5.1 超声振动

超声波作用于液体会产生声流和空化效应。声流是由于液体材料吸收声波振荡而产生的动量传导所驱动的稳定流动；空化是一种动态现象，是由于超声作用下液体内局部产生的负压会产生气泡或空穴，随周围介质的振动不断运动、长大，最终突然破裂，破裂时周围液体突然冲入空穴处会产生高温、高压[48,146]。超声场作用于LAM中时，声流和空化效应会对熔池熔体流动和晶体生长产生较大影响。下面对超声振动辅助SLM和LDED工艺分别进行阐述。

由于SLM过程需要在密闭无氧腔体中完成，将超声装置与SLM设备集成具有挑战性，相关研究较少。现有研究表明超声振动虽然可在一定程度上调控SLM冶金过程，但对制件力学性能提升效果有限。Guo等[147]得出2 kHz超声场降低了316L位错密度、减缓应力、缓解裂纹、细化晶粒尺寸并促进柱状晶向等轴晶转变，样品极限拉伸强度略有提升(4%)。Yan等[148]同样也发现超声振动会促进GH5188高温合金晶粒细化和等轴化转变，但合金力学性能仅得到轻微改善。

研究学者针对超声场辅助LDED工艺已开展广泛的研究，结果表明超声振动有利于改善成形过程中的冶金缺陷问题，例如Cong等[149]发现超声波在熔体中产生强烈搅拌，缓解了AISI630顶面的球化效应，改善了表面粗糙度，而且超声波诱导的声流和空化作用可打破气体形成的空隙，减少甚至消除了气孔、空洞及微裂纹缺陷，降低了残余应力。超声振动还可调控溶质分配行为和相分布特征，例如：Niu等[150]发现超声场诱导产生的空化气泡破裂产生瞬时高温高压，促进TiC/Ti6Al4V复合涂层中未融化TiC含量降低，且声流加速熔体流动，改善原生TiC在基体中分布的均匀性，涂层显微硬度提高了26%左右；Wu等[151]发现超声振动提高了熔池冷却速率，抑制IN718/Ti6Al4V复合材料中β-Ti相向Ti_2Ni转变，且在超声空化效应的高强度冲击下，粗长链Ti_2Ni相破碎，转变为细小颗粒状形态，在声流作用下均匀分布，有效改善了复合材料的脆性晶间断裂，弯曲强度提高30%以上，超声辅助熔池凝固行为如图11(a)所示。最为关键的是，超声振动可促进晶粒细化和等轴化转变，提升制件综合力学性能，例如：Gorunov[152]发现超声振动促进Ti6Al4V等轴晶区形成和晶粒细化，抗疲劳性能提高50%；Wang等[153]发现IN718晶粒尺寸随超声波频率的增加而减小，Laves相由长条柱状变为颗粒状，当超声频率超过25 kHz时空化效应减弱，会导致孔隙率增加，不同超声频率下样品微观形貌如图11(b)所示；Todaro等[154]得出20 kHz超声降低了316L熔池温度梯度，扩大成分过冷区，从而创造了有利于晶核形成和生长的条件，实现了晶粒细化和等轴化转变，样品EBSD结果如图11(c)所示；Chen等[155]也发现20 kHz超声场使CoCrFeMnNi高熵合金平均晶粒尺寸从140 μm减小到44 μm，拉伸强度提升了17%左右，细小等轴晶的形成与超声场促进枝晶破碎成为异质形核点和凝固前沿成分过冷的增加有关；Yao等[156]得出超声场加快了316L熔池热对流，减小温度梯度，凝固界面前沿成分过冷增加，促进晶粒形核和细小等轴晶形成，样品微观形貌如图11(d)所示。

因此，超声振动在熔池中诱导产生的声流加速熔体流动，减少气孔、空隙等冶金缺陷，改善LDED工艺

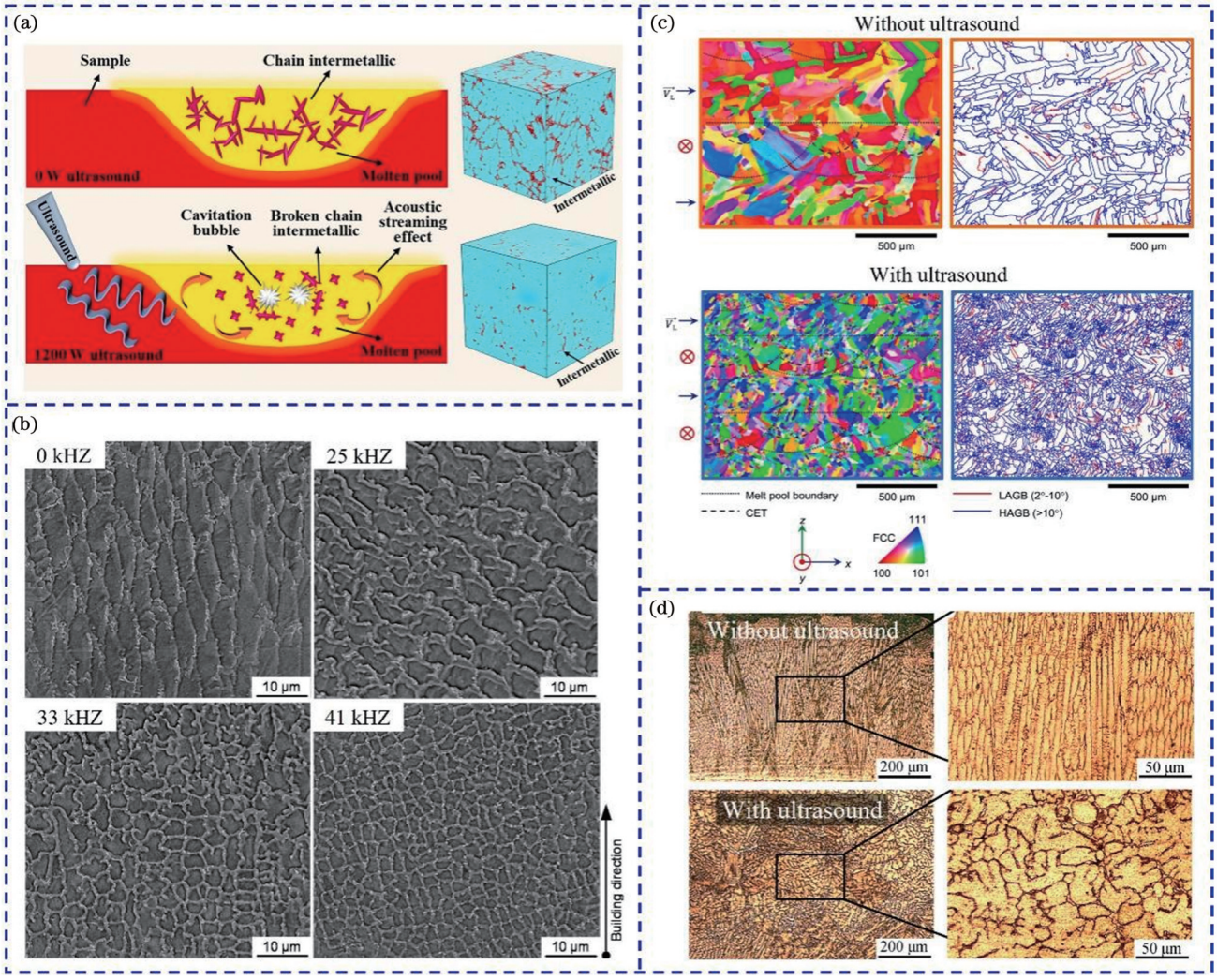

图 11 超声振动辅助激光增材制造技术。(a)超声辅助 LDED 工艺熔池凝固行为[151];(b)不同超声频率(0、25、33、41 kHz)下 LDED 制备 IN718 微观形貌[153];(c)无超声场和 20 kHz 超声场辅助 LDED 制备 316L 合金 EBSD 图[154];(d)无超声场和超声场辅助 LDED 制备 316L 不锈钢 OM 图[156]

Fig. 11 Ultrasonic vibration-assisted laser additive manufacturing technology. (a) Solidification behavior of melt pool in ultrasonic assisted LDED[151]; (b) micro-morphology of IN718 prepared by LDED at different ultrasonic frequencies (0, 25, 33, 41 kHz)[153]; (c) EBSD image of 316L alloy prepared by LDED with 20 kHz and without ultrasonic field[154]; (d) OM diagram of 316L stainless steel fabricated by LDED with and without ultrasonic field assistance[156]

成形部件表面粗糙度,还可进一步调控溶质分配行为和相分布特征;空化效应降低熔池温度梯度,扩大凝固前沿成分过冷区,并诱导枝晶破碎增加形核位点,促进晶粒细化和等轴化转变,提升制件综合力学性能。

5.2 超声冲击强化

超声冲击强化是通过高频超声波驱动冲击针撞击金属工件表面,使其在一定深度内发生塑性变形,改变原始微观结构特征和晶体形态,从而实现强化效果[157]。金属激光增材制造样品仅仅依靠激光熔融使层与层之间堆积成形,缺乏机械压实,导致制件整体性能普遍低于传统锻造零件。原位超声冲击强化通过机械外力随激光熔融过程对成形样品进行层层高频撞击,是提升 LAM 制件力学性能的有效方法,相关研究已获得积极效果。

原位超声冲击强化可有效改善残余应力状态,减少 LAM 成形过程中的冶金缺陷,例如:Zhang 等[158]发现原位超声冲击强化使 SLM 制备 Ti6Al4V 中残余应力从 176.3 MPa 降低至 49.9 MPa,由于其引起的塑性变形和 SLM 快速加热所产生的再结晶,缺陷被有效减少甚至消除;Wang 等[159]发现 75 N 超声冲击力可使 LDED 成形难焊接 IN100 的裂纹密度降低到接近零,表面质量显著改善,工艺原理和超声冲击前后形貌对比如图 12(a)和图 12(b)所示;Zhou 等[160]利用有限元分析揭示了超声冲击使 LDED 成形 304 不锈钢的残余应力状态从拉应力转变为压应力,有利于合金疲劳性能的改善。原位超声冲击还可通过增加位错密度和晶格畸变,阻碍位错滑移,增强合金的强度和硬度,例如:Wang 等[161]发现超声冲击提高了 LDED 制备 Ti6Al4V

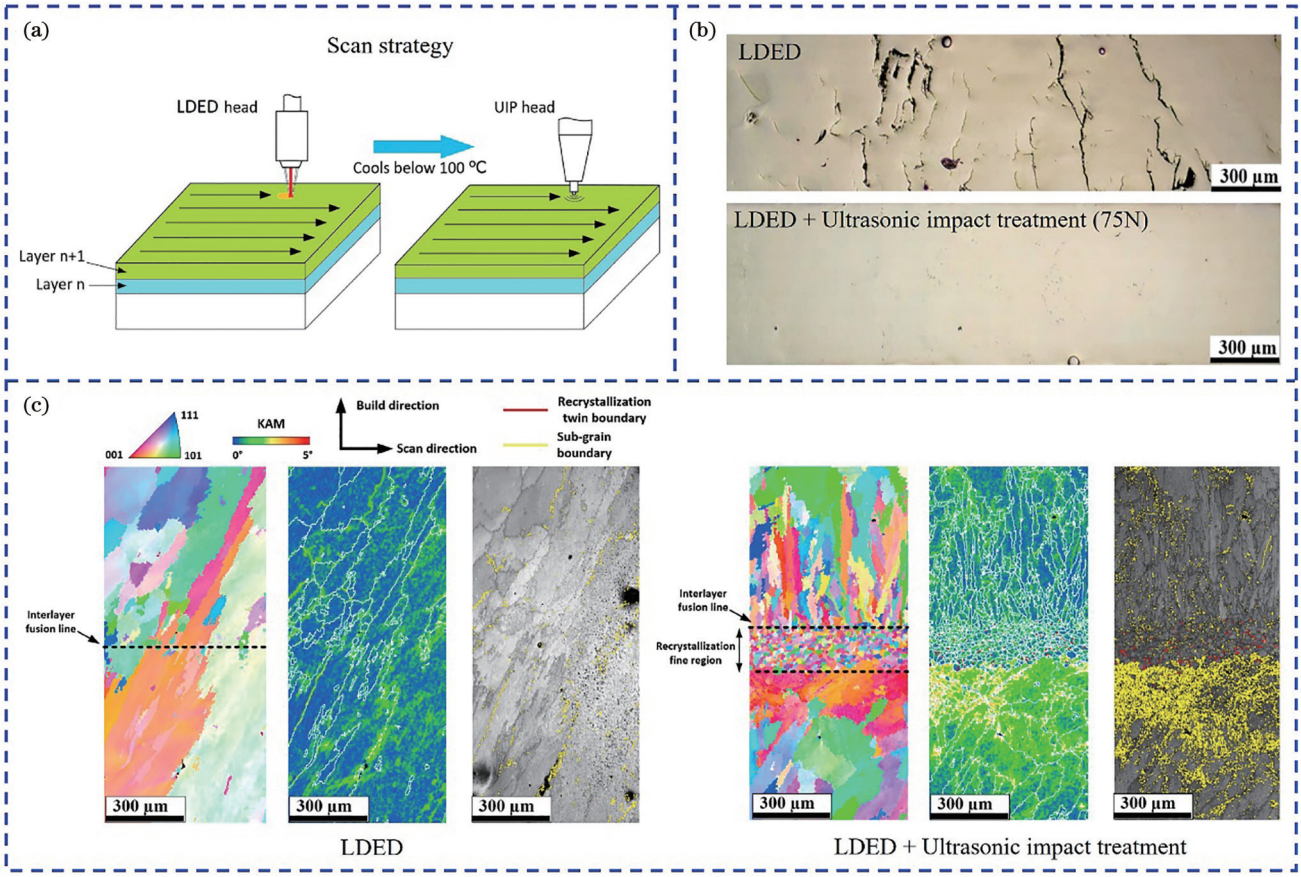

图 12 超声冲击辅助激光增材制造技术。(a) LDED+超声冲击工艺扫描策略[159];(b) 75 N超声冲击和未超声冲击LDED成形IN100高温合金形貌图[159];(c)超声冲击前后LDED成形IN718合金的反极图面分布图(IPF)、局部取向差(KAM)和晶界(GB)分布[165]

Fig. 12 Ultrasonic impact-assisted laser additive manufacturing technology. (a) Scan strategy[159]; (b) microscope images of LDED-fabricated IN100 superalloy with and without 75 N ultrasonic impact[159]; (c) inverse pole figure (IPF) mappings, kernel average misorientation (KAM), and grain boundary (GB) distribution of LDED-fabricated IN718 with and without ultrasonic impact[165]

的位错密度和α/α′相晶格畸变,促进保留β晶粒中析出纳米级α相,屈服强度提高了41.2%;Wang等[162]得出超声冲击促使LDED成形IN718中产生大量孪晶和动态再结晶组织,表面区域的显微硬度增加了30%,内部增加了20%;Xu等[163]发现超声冲击导致LDED成形哈氏合金X中产生位错堆积阻碍晶粒运动,样品在750 ℃下的屈服强度提高超过30%。更关键的是,超声冲击会促进晶粒细化,提升制件整体性能,例如:Wei等[164]利用有限元分析得出超声冲击可提高LDED熔池中的最大流速,通过增大冷却速率促进柱状晶向等轴晶过渡,并细化凝固过程中沉积层的晶粒大小;Wang等[165]发现超声冲击引起的显著塑性变形会引发LDED成形IN718中动态再结晶,形成细小的等轴层间带,屈服强度和拉伸模量分别提高了28%和67%,超声冲击前后样品层间组织对比如图12(c)所示。因此,原位超声冲击强化是缓解LAM成形样品残余应力,细化组织并提高制件整体力学性能的有效方式。

综上所述,原位超声振动和超声冲击是两种基于超声外场调控激光增材制造冶金过程的有效方式。超声振动产生的声流效应可促进熔池中溶质均匀分布,减少偏析,空化可诱导枝晶破碎增加形核位点,促进晶粒细化和等轴化转变,提高制件的整体性能;超声冲击主要是通过超声场转化为机械撞击使成形样品产生塑性变形,缓解制件中的残余应力,细化晶粒并消除孔隙等冶金缺陷。然而超声冲击过程中样品受到机械冲击和超声振动双重作用,制件内部不同深度受作用程度不同,可能会加剧组织和性能各向异性。SLM需要在密闭腔体中进行,原位超声辅助技术集成难度大,且现有研究表明对性能影响有限,因此原位超声振动和超声冲击在适合大尺寸零件制备的LDED中具有较大工程应用和科学研究意义。

6 总结与展望

激光增材制造技术因高柔性、成形周期短等优点在很多领域备受青睐,但经大量不同金属材料的成形实验发现,高斯激光中心峰值能量密度大,易使熔池中产生高温度梯度和相对紊乱的流场,造成气孔、飞溅、残余应力、裂纹等缺陷,阻碍了其应用与发展。从工艺角度上进行激光矫形和施加辅助外场可从源头上对激

光增材制造过程进行调控，克服其目前面临的瓶颈问题。本文综述了不同矫形激光（平顶激光、反高斯激光、贝塞尔激光、椭圆形激光和离焦激光）和热场、磁场、超声场辅助金属激光增材制造技术的国内外研究进展，阐明了矫形光束及外场对熔池温度场和流场以及不同成形材料的晶体生长、组织和性能的影响规律。主要结论和需进一步关注的发展方向如下。

1）矫形激光研究表明平顶光束、反高斯光束、贝塞尔光束和离焦光束均可使传统高斯激光中心峰值能量降低，减小熔池温度梯度，缓解气孔、裂纹等缺陷产生，并且可改善熔池形态，有利于晶体外延生长，在制备定向晶、单晶等特殊组织上具有优势。而椭圆形光束可促进晶粒细化和等轴化转变，有利于消除各向异性特征。然而，矫形激光增材制造成形金属构件目前还处于起步探索阶段，相关研究有限，矫形光束与材料的作用机理还需深入研究。以下三个方面值得关注：第一，可通过基于热力学、流体力学等的数值模拟探究不同能量分布的矫形激光熔池中的温度场和流场分布特征，明晰晶体生长规律，同时借助同步辐射X射线高速成像、中子衍射成像等技术探究新型热源下匙孔演变特征、熔池形态及缺陷产生的过程；第二，进行矫形激光增材制造工艺参数优化，探究激光功率、扫描速度、层厚、扫描策略、搭接宽度等对材料组织和性能的影响；第三，矫形光路系统还不成熟，需探究更加灵活且与现有增材制造设备适配度高的光束矫形方案。由于不同能量分布激光对材料作用规律不同，未来可通过空间光调制器等特殊装置实时调整光束能量分布，从而达到定制金属微观组织的目的，实现结构-功能一体化成形。

2）热场通过热量传递降低激光增材制造过程中熔池的温度梯度，延长熔体凝固时间，可减少元素偏析，改善成形构件中的残余应力和裂纹。基底预热工艺简单，但预热温度有限，易造成成形构件沿高度方向的组织和性能出现差异，未来可探究利用这一差异实现沿构建方向的功能梯度材料的制备。电磁感应加热可对构建整体均匀预热，且可实现的加热温度高，但工艺还不成熟，熔池凝固过程除受热场影响外还有磁场的作用，未来需通过多物理场模拟和实验对电磁感应加热与熔池凝固间的作用机理进行深入研究。激光同步预热能量利用率高，但预热激光的功率、能量分布、扫描速度以及与熔化激光的时间间隔等对不同成形样品组织和性能的影响还需更深入研究。

3）磁场作用下熔池中产生的洛伦兹力和热电磁对流会改变熔体流动过程，促使枝晶破碎而增加形核位点，有利于实现晶粒细化和等轴化转变，提升合金力学性能。交变磁场由于涡流效应会使成形样品内部产生热量，与熔池作用过程较为复杂且研究有限，未来可结合多物理场数值模拟进一步探究磁场方向、频率、功率等对不同金属材料的影响规律，揭示交变磁场对熔池凝固的作用机理。

4）超声场可诱导熔池中产生声流和空化效应，不仅能调控熔体的流动过程，抑制偏析，而且能促进晶粒细化，改善样品中的残余应力。不同于热场和磁场，超声场会使成形构件中产生机械振动的动能，需进一步探究其对飞溅、匙孔和熔池形态的影响，以及合金中位错、层错、孪晶等微观特征的作用机理。

不同形式的场对熔池金属凝固过程作用机理不同，目前的研究大多只针对单一场，未来可进一步探索多场同步辅助激光增材制造技术对不同成形材料的作用规律，拓宽金属激光增材制造技术在不同领域的应用前景。

参 考 文 献

[1] 顾冬冬, 张红梅, 陈洪宇, 等. 航空航天高性能金属材料构件激光增材制造[J]. 中国激光, 2020, 47(5): 0500002.
Gu D D, Zhang H M, Chen H Y, et al. Laser additive manufacturing of high-performance metallic aerospace components [J]. Chinese Journal of Lasers, 2020, 47(5): 0500002.

[2] Gu D D, Shi X Y, Poprawe R, et al. Material-structure-performance integrated laser-metal additive manufacturing[J]. Science, 2021, 372(6545): eabg1487.

[3] Liu Y B, Li J K, Xu K, et al. An optimized scanning strategy to mitigate excessive heat accumulation caused by short scanning lines in laser powder bed fusion process[J]. Additive Manufacturing, 2022, 60: 103256.

[4] Tofail S A M, Koumoulos E P, Bandyopadhyay A, et al. Additive manufacturing: scientific and technological challenges, market uptake and opportunities[J]. Materials Today, 2018, 21(1): 22-37.

[5] Li J J, Ouyang D, Li J K, et al. New insight into the strengthening mechanism of $AlCoCrFeNi_{2.1}$ eutectic high-entropy alloy with dual-phase nanolamellar structures achieved via laser powder bed fusion [J]. Materials Science and Engineering: A, 2023, 887: 145784.

[6] Li J K, Cheng T, Liu Y B, et al. Simultaneously enhanced strength and ductility of Cu-15Ni-8Sn alloy with periodic heterogeneous microstructures fabricated by laser powder bed fusion[J]. Additive Manufacturing, 2022, 54: 102726.

[7] Tan C L, Weng F, Sui S, et al. Progress and perspectives in laser additive manufacturing of key aeroengine materials[J]. International Journal of Machine Tools and Manufacture, 2021, 170: 103804.

[8] Haberland C, Elahinia M, Walker J M, et al. On the development of high quality NiTi shape memory and pseudoelastic parts by additive manufacturing[J]. Smart Material Structures, 2014, 23 (10): 104002.

[9] Babacan N, Pauly S, Gustmann T. Laser powder bed fusion of a superelastic Cu-Al-Mn shape memory alloy[J]. Materials & Design, 2021, 203: 109625.

[10] Ferretto I, Kim D, Della Ventura N M, et al. Laser powder bed fusion of a Fe-Mn-Si shape memory alloy[J]. Additive Manufacturing, 2021, 46: 102071.

[11] 谢寅, 滕庆, 沈沐宇, 等. 多激光粉床熔融成形GH3536合金搭接区域组织与性能特征研究[J]. 中国激光, 2023, 50(8): 0802303.
Xie Y, Teng Q, Shen M Y, et al. Study on microstructure and properties of overlap region of GH3536 alloy processed by multi-laser powder bed fusion[J]. Chinese Journal of Lasers, 2023, 50 (8): 0802303.

[12] 李继康, 张振武, 杨源祺, 等. 激光选区熔化DD91镍基单晶高温合金的单道形貌、晶体取向和微观组织[J]. 中国激光, 2022, 49 (14): 1402103.
Li J K, Zhang Z W, Yang Y Q, et al. Single-track morphology, crystal orientation and microstructure of DD91 nickel-based single

crystal superalloy fabricated by selective laser melting[J]. Chinese Journal of Lasers, 2022, 49(14): 1402103.

[13] Xie Y, Teng Q, Shen M Y, et al. The role of overlap region width in multi-laser powder bed fusion of Hastelloy X superalloy [J]. Virtual and Physical Prototyping, 2023, 18(1): e2142802.

[14] Zhao D L, Yu K D, Sun T F, et al. Material-structure-function integrated additive manufacturing of degradable metallic bone implants for load-bearing applications[J]. Advanced Functional Materials, 2023, 33(16): 2213128.

[15] 张志, 宋波, 王晓波, 等. 吸能的力学超材料设计与增材制造研究现状及趋势[J]. 中国激光, 2022, 49(14): 1402301.
Zhang Z, Song B, Wang X B, et al. Research status and trend of design and addictive manufacturing for mechanical metamaterials with energy absorption[J]. Chinese Journal of Lasers, 2022, 49 (14): 1402301.

[16] Svetlizky D, Das M, Zheng B L, et al. Directed energy deposition (DED) additive manufacturing: physical characteristics, defects, challenges and applications[J]. Materials Today, 2021, 49: 271-295.

[17] Zhang Z Y, Li J K, Cheng T, et al. Simultaneously enhanced strength and ductility of $AlSi_7Mg$ alloy fabricated by laser powder bed fusion with on-line static magnetic field[J]. Virtual and Physical Prototyping, 2023, 18(1): e2161918.

[18] Cai C, Wu X, Liu W, et al. Selective laser melting of near-α titanium alloy Ti-6Al-2Zr-1Mo-1V: Parameter optimization, heat treatment and mechanical performance[J]. Journal of Materials Science & Technology, 2020, 57: 51-64.

[19] Dang M Z, Xiang H H, Li J K, et al. Laser powder bed fusion of full martensite Cu-Al-Mn-Ti alloy with good superelasticity and shape memory effect[J]. Materials Science and Engineering: A, 2023, 884: 145475.

[20] 田健, 魏青松, 朱文志, 等. Cu-Al-Ni-Ti合金激光选区成形工艺及其力学性能[J]. 中国激光, 2019, 46(3): 0302001.
Tian J, Wei Q S, Zhu W Z, et al. Selective laser melting process and mechanical properties of Cu-Al-Ni-Ti alloy[J]. Chinese Journal of Lasers, 2019, 46(3): 0302001.

[21] Teng Q, Li S, Wei Q S, et al. Investigation on the influence of heat treatment on Inconel 718 fabricated by selective laser melting: microstructure and high temperature tensile property[J]. Journal of Manufacturing Processes, 2021, 61: 35-45.

[22] 沈沐宇, 谢寅, 李继康, 等. 激光功率对双激光粉末床熔融GH3536合金搭接区组织和性能的影响[J]. 中国激光, 2023, 50 (24): 2402301.
Shen M Y, Xie Y, Li J K, et al. Influence of laser power on microstructure and properties of overlap region in dual-laser powder bed fusion of GH3536 superalloy[J]. Chinese Journal of Lasers, 2023, 50(24): 2402301.

[23] Gao C D, Li S, Liu L, et al. Dual alloying improves the corrosion resistance of biodegradable Mg alloys prepared by selective laser melting[J]. Journal of Magnesium and Alloys, 2021, 9(1): 305-316.

[24] Li W, Li J K, Duan X Y, et al. Dislocation-induced ultra-high strength in a novel steel fabricated using laser powder-bed-fusion [J]. Materials Science and Engineering: A, 2022, 832: 142502.

[25] 李虎, 赵伟江, 李瑞迪, 等. 增材制造马氏体时效钢的研究进展[J]. 中国激光, 2022, 49(14): 1402102.
Li H, Zhao W J, Li R D, et al. Progress on additive manufacturing of maraging steel[J]. Chinese Journal of Lasers, 2022, 49(14): 1402102.

[26] Wei Q S, Xie Y, Teng Q, et al. Crack types, mechanisms, and suppression methods during high-energy beam additive manufacturing of nickel-based superalloys: a review[J]. Chinese Journal of Mechanical Engineering: Additive Manufacturing Frontiers, 2022, 1(4): 100055.

[27] Huang Y Z, Fleming T G, Clark S J, et al. Keyhole fluctuation and pore formation mechanisms during laser powder bed fusion additive manufacturing[J]. Nature Communications, 2022, 13: 1170.

[28] Mostafaei A, Zhao C, He Y N, et al. Defects and anomalies in powder bed fusion metal additive manufacturing[J]. Current Opinion in Solid State and Materials Science, 2022, 26(2): 100974.

[29] Yang G, Xie Y L, Zhao S, et al. Quality control: internal defects formation mechanism of selective laser melting based on laser-powder-melt pool interaction: a review[J]. Chinese Journal of Mechanical Engineering: Additive Manufacturing Frontiers, 2022, 1(3): 100037.

[30] Guo L P, Wang H Z, Liu H J, et al. Understanding keyhole induced-porosities in laser powder bed fusion of aluminum and elimination strategy[J]. International Journal of Machine Tools and Manufacture, 2023, 184: 103977.

[31] Li J J, Ouyang D, Wang Q H, et al. Achieving superior tensile strength of $CoCrFeNiTi_{0.3}$ high-entropy alloy via *in situ* laser powder bed fusion of CoCrFeNi and Ti[J]. Materials Science and Engineering: A, 2023, 886: 145649.

[32] Guo C, Yu Z R, Hu X G, et al. Y_2O_3 nanoparticles decorated IN738LC superalloy manufactured by laser powder bed fusion: cracking inhibition, microstructures and mechanical properties[J]. Composites Part B: Engineering, 2022, 230: 109555.

[33] Wilms M B, Rittinghaus S K, Goßling M, et al. Additive manufacturing of oxide-dispersion strengthened alloys: materials, synthesis and manufacturing[J]. Progress in Materials Science, 2023, 133: 101049.

[34] Li J K, Zhang Z W, Xu W H, et al. Hot isostatic pressing of Cu-15Ni-8Sn alloy with suppressed Sn macro-segregation and enhanced mechanical properties[J]. Materials Science and Engineering: A, 2022, 855: 143866.

[35] Cai C, Gao X Y, Teng Q, et al. Hot isostatic pressing of a near α-Ti alloy: temperature optimization, microstructural evolution and mechanical performance evaluation[J]. Materials Science and Engineering: A, 2021, 802: 140426.

[36] Teng Q, Wei Q S, Xue P J, et al. Effects of processing temperatures on FGH4097 superalloy fabricated by hot isostatic pressing: microstructure evolution, mechanical properties and fracture mechanism[J]. Materials Science and Engineering: A, 2019, 739: 118-131.

[37] 孙闪闪, 滕庆, 程坦, 等. 热处理对激光选区熔化GH3536合金组织演变规律的影响研究[J]. 机械工程学报, 2020, 56(21): 208-218.
Sun S S, Teng Q, Cheng T, et al. Influence of heat treatment on microstructure evolution of GH3536 superalloy fabricated by selective laser melting[J]. Journal of Mechanical Engineering, 2020, 56(21): 208-218.

[38] Sun S S, Teng Q, Xie Y, et al. Two-step heat treatment for laser powder bed fusion of a nickel-based superalloy with simultaneously enhanced tensile strength and ductility[J]. Additive Manufacturing, 2021, 46: 102168.

[39] Hu Y B. Recent progress in field-assisted additive manufacturing: materials, methodologies, and applications[J]. Materials Horizons, 2021, 8(3): 885-911.

[40] 林勇, 胡家升. 激光光束的整形技术[J]. 激光杂志, 2008, 29(6): 1-4.
Lin Y, Hu J S. Laser beam shaping techniques[J]. Laser Journal, 2008, 29(6): 1-4.

[41] 龙雨, 黄玮, 郭兴, 等. 非传统激光束激光选区熔化3D打印的研究现状及展望[J]. 航空制造技术, 2022, 65(1/2): 34-48.
Long Y, Huang W, Guo X, et al. Selective laser melting 3D printing using non-traditional laser beam: a review[J]. Aeronautical Manufacturing Technology, 2022, 65(1/2): 34-48.

[42] Bi J, Wu L K, Li S D, et al. Beam shaping technology and its application in metal laser additive manufacturing: a review[J]. Journal of Materials Research and Technology, 2023, 26: 4606-4628.

[43] Gussone J, Rackel M W, Tumminello S, et al. Microstructure

formation during laser powder bed fusion of Ti-22Al-25Nb with low and high pre-heating temperatures[J]. Materials & Design, 2023, 232: 112154.

[44] Qin S Y, Saewe J, Kunz J, et al. Influence of preheating temperature on microstructure evolution and hardness of high-speed steel AISI M50 processed by laser powder bed fusion[J]. Steel Research International, 2023, 94(6): 2200784.

[45] Wang W H, Lin W H, Yang R, et al. Mesoscopic evolution of molten pool during selective laser melting of superalloy Inconel 738 at elevating preheating temperature[J]. Materials & Design, 2022, 213: 110355.

[46] Guo S, Sui S, Wang M, et al. Simultaneously optimizing the strength and ductility of high-entropy alloys by magnetic field-assisted additive manufacturing[J]. Journal of Alloys and Compounds, 2023, 947: 169688.

[47] Zhang B, Shirvani K, Taheri M, et al. Effect of TiC and magnetic field on microstructure and mechanical properties of IN738 superalloy processed by selective laser melting[J]. Journal of Materials Engineering and Performance, 2024, 33: 3494-3509.

[48] 吴文华, 翟薇, 王建元, 等. 超声场中液体材料的空化和声流动力学研究进展[J]. 中国科学: 技术科学, 2023, 53(1): 2-27.
Wu W H, Zhai W, Wang J Y, et al. Progress of cavitation and acoustic streaming dynamics of liquid materials within ultrasonic field[J]. Science China Technological Sciences, 2023, 53(1): 2-27.

[49] Kosiba K, Gustmann T, Kim J T, et al. Experimental cooling rates during high-power laser powder bed fusion at varying processing conditions[J]. Journal of Alloys and Compounds, 2023, 967: 171773.

[50] Galbusera F, Caprio L, Previtali B, et al. The influence of novel beam shapes on melt pool shape and mechanical properties of LPBF produced Al-alloy[J]. Journal of Manufacturing Processes, 2023, 85: 1024-1036.

[51] Chen B, Bian Y H, Li Z Y, et al. Effect of laser beam profile on thermal transfer, fluid flow and solidification parameters during laser-based directed energy deposition of Inconel 718[J]. Materials, 2023, 16(12): 4221.

[52] Gil E, Mancisidor A M, Iturrioz A, et al. Cracking susceptibility of maraging parts manufactured by laser powder bed fusion additive manufacturing: study on the powder characteristics and baseplate preheating influence[J]. Powder Metallurgy, 2023, 66(5): 416-426.

[53] Zhou L, Chen S Y, Jia W M, et al. Effects of preheating-ultrasonic synergistic on the microstructure and strength-ductility of 24CrNiMoY alloy steel by laser directed energy deposition[J]. Materials Science and Engineering: A, 2023, 863: 144463.

[54] Zhou Y, Qu W Y, Zhou F, et al. Thermo-fluid flow behavior of the IN718 molten pool in the laser directed energy deposition process under magnetic field[J]. Rapid Prototyping Journal, 2023, 29(3): 460-473.

[55] Frieden B R. Lossless conversion of a plane laser wave to a plane wave of uniform irradiance[J]. Applied Optics, 1965, 4(11): 1400-1403.

[56] Sow M C, de Terris T, Castelnau O, et al. Influence of beam diameter on laser powder bed fusion (L-PBF) process[J]. Additive Manufacturing, 2020, 36: 101532.

[57] Wang K, Xie D Q, Lü F, et al. Stability of molten pool and microstructure evolution of Ti-6Al-4V during laser powder bed fusion with a flat-top beam[J]. Additive Manufacturing, 2023, 75: 103756.

[58] Belay G Y, Kinds Y, Goossens L, et al. Dynamic optical beam shaping system to generate Gaussian and top-hat laser beams of various sizes with circular and square footprint for additive manufacturing applications[J]. Procedia CIRP, 2022, 111: 75-80.

[59] Huang S, Narayan R L, Tan J H K, et al. Resolving the porosity-unmelted inclusion dilemma during *in situ* alloying of $Ti_{34}Nb$ via laser powder bed fusion[J]. Acta Materialia, 2021, 204: 116522.

[60] Yuan W H, Chen H, Li S, et al. Understanding of adopting flat-top laser in laser powder bed fusion processed Inconel 718 alloy: simulation of single-track scanning and experiment[J]. Journal of Materials Research and Technology, 2022, 16: 1388-1401.

[61] Wang Y C, Shi J. Developing very strong texture in a nickel-based superalloy by selective laser melting with an ultra-high power and flat-top laser beam[J]. Materials Characterization, 2020, 165: 110372.

[62] Jodi D E, Kitashima T, Koizumi Y, et al. Manufacturing single crystals of pure nickel via selective laser melting with a flat-top laser beam[J]. Additive Manufacturing Letters, 2022, 3: 100066.

[63] Montero-Sistiaga M L, Godino-Martinez M, Boschmans K, et al. Microstructure evolution of 316L produced by HP-SLM (high power selective laser melting)[J]. Additive Manufacturing, 2018, 23: 402-410.

[64] Montero-Sistiaga M L, Pourbabak S, Van Humbeeck J, et al. Microstructure and mechanical properties of Hastelloy X produced by HP-SLM (high power selective laser melting) [J]. Materials & Design, 2019, 165: 107598.

[65] Liu Y, Wang Y C, Savinov R, et al. Epitaxial growth of a single-crystal nickel-based superalloy during laser melting with high-power flat-top laser[J]. Optics & Laser Technology, 2021, 144: 107444.

[66] Jodi D E, Kitashima T, Singh A, et al. High-temperature microstructural stability of pure Ni fabricated by laser powder bed fusion using Gaussian and flat-top beam profiles[J]. Materials Characterization, 2023, 200: 112897.

[67] Jodi D E, Kitashima T, Watanabe M. Effect of scan strategy on the formation of a pure nickel single-crystal structure using a flat-top laser beam via laser powder bed fusion[J]. Science and Technology of Advanced Materials, 2023, 24(1): 2201380.

[68] Liu M N, Wei K W, Yue X Z, et al. High power laser powder bed fusion of AlSi10Mg alloy: effect of laser beam mode[J]. Journal of Alloys and Compounds, 2022, 909: 164779.

[69] Okunkova A A, Peretyagin P Y, Podrabinnik P A, et al. Development of laser beam modulation assets for the process productivity improvement of selective laser melting[J]. Procedia IUTAM, 2017, 23: 177-186.

[70] Pilz S, Gustmann T, Günther F, et al. Controlling the Young's modulus of a ß-type Ti-Nb alloy via strong texturing by LPBF[J]. Materials & Design, 2022, 216: 110516.

[71] Meng G R, Gong Y D, Zhang J D, et al. Microstructure and mechanical properties of Inconel 718 thin walls prepared by laser direct energy deposition and selective laser melting[J]. Thin-Walled Structures, 2023, 193: 111284.

[72] Chen Y, Guo Y B, Xu M J, et al. Study on the element segregation and Laves phase formation in the laser metal deposited IN718 superalloy by flat top laser and Gaussian distribution laser [J]. Materials Science and Engineering: A, 2019, 754: 339-347.

[73] Wang A, Wei Q L, Luo S, et al. Blue laser directed energy deposition of aluminum with synchronously enhanced efficiency and quality[J]. Additive Manufacturing Letters, 2023, 5: 100127.

[74] Wang A, Wei Q L, Tang Z J, et al. Effects of processing parameters on pore defects in blue laser directed energy deposition of aluminum by in and *ex situ* observation[J]. Journal of Materials Processing Technology, 2023, 319: 118068.

[75] Kim C K, Jeong J I, Choi S G, et al. High-throughput directed energy deposition process with an optimized scanning nozzle[J]. Journal of Materials Processing Technology, 2021, 295: 117165.

[76] Cheng M P, Xiao X F, Luo G Y, et al. Effect of laser intensity profile on the microstructure and texture of Inconel 718 superalloy fabricated by direct energy deposition[J]. Journal of Materials Research and Technology, 2022, 18: 2001-2012.

[77] Wang R, Wang J, Cao T W, et al. Microstructure characteristics of a René N5 Ni-based single-crystal superalloy prepared by laser-directed energy deposition[J]. Additive Manufacturing, 2023, 61: 103363.

[78] Cloots M, Uggowitzer P J, Wegener K. Investigations on the microstructure and crack formation of IN738LC samples processed by selective laser melting using Gaussian and doughnut profiles[J]. Materials & Design, 2016, 89: 770-784.

[79] Wischeropp T M, Tarhini H, Emmelmann C. Influence of laser beam profile on the selective laser melting process of AlSi10Mg[J]. Journal of Laser Applications, 2020, 32(2): 022059.

[80] Grigoriev S N, Gusarov A V, Metel A S, et al. Beam shaping in laser powder bed fusion: Péclet number and dynamic simulation[J]. Metals, 2022, 12(5): 722.

[81] Duocastella M, Arnold C B. Bessel and annular beams for materials processing[J]. Laser & Photonics Reviews, 2012, 6(5): 607-621.

[82] Grünewald J, Gehringer F, Schmöller M, et al. Influence of ring-shaped beam profiles on process stability and productivity in laser-based powder bed fusion of AISI 316L[J]. Metals, 2021, 11(12): 1989.

[83] Nahr F, Bartels D, Rothfelder R, et al. Influence of novel beam shapes on laser-based processing of high-strength aluminium alloys on the basis of EN AW-5083 single weld tracks[J]. Journal of Manufacturing and Materials Processing, 2023, 7(3): 93.

[84] Tumkur T U, Voisin T, Shi R P, et al. Nondiffractive beam shaping for enhanced optothermal control in metal additive manufacturing[J]. Science Advances, 2021, 7(38): eabg9358.

[85] Roehling T T, Wu S S Q, Khairallah S A, et al. Modulating laser intensity profile ellipticity for microstructural control during metal additive manufacturing[J]. Acta Materialia, 2017, 128: 197-206.

[86] Roehling T T, Shi R P, Khairallah S A, et al. Controlling grain nucleation and morphology by laser beam shaping in metal additive manufacturing[J]. Materials & Design, 2020, 195: 109071.

[87] Shi R P, Khairallah S A, Roehling T T, et al. Microstructural control in metal laser powder bed fusion additive manufacturing using laser beam shaping strategy[J]. Acta Materialia, 2020, 184: 284-305.

[88] Zhong Q, Wei K W, Lu Z A, et al. High power laser powder bed fusion of Inconel 718 alloy: effect of laser focus shift on formability, microstructure and mechanical properties[J]. Journal of Materials Processing Technology, 2023, 311: 117824.

[89] Nie X J, Chen Z, Qi Y, et al. Effect of defocusing distance on laser powder bed fusion of high strength Al-Cu-Mg-Mn alloy[J]. Virtual and Physical Prototyping, 2020, 15(3): 325-339.

[90] Soylemez E. High deposition rate approach of selective laser melting through defocused single bead experiments and thermal finite element analysis for Ti-6Al-4V[J]. Additive Manufacturing, 2020, 31: 100984.

[91] Patel S, Chen H X, Vlasea M, et al. The influence of beam focus during laser powder bed fusion of a high reflectivity aluminium alloy: AlSi10Mg[J]. Additive Manufacturing, 2022, 59: 103112.

[92] McLouth T D, Bean G E, Witkin D B, et al. The effect of laser focus shift on microstructural variation of Inconel 718 produced by selective laser melting[J]. Materials & Design, 2018, 149: 205-213.

[93] Bean G E, Witkin D B, McLouth T D, et al. Effect of laser focus shift on surface quality and density of Inconel 718 parts produced via selective laser melting[J]. Additive Manufacturing, 2018, 22: 207-215.

[94] Zhao Y H, Sun W Y, Wang Q, et al. Effect of beam energy density characteristics on microstructure and mechanical properties of nickel-based alloys manufactured by laser directed energy deposition[J]. Journal of Materials Processing Technology, 2023, 319: 118074.

[95] Chen X Y, Xie X L, Wu H, et al. *In-situ* control of residual stress and its distribution in a titanium alloy additively manufactured by laser powder bed fusion[J]. Materials Characterization, 2023, 201: 112953.

[96] Lu X F, Lin X, Chiumenti M, et al. Residual stress and distortion of rectangular and S-shaped Ti-6Al-4V parts by directed energy deposition: modelling and experimental calibration[J]. Additive Manufacturing, 2019, 26: 166-179.

[97] Polozov I, Kantyukov A, Popovich V, et al. Microstructure and mechanical properties of TiAl-based alloy produced by selective laser melting[C]//29th International Conference on Metallurgy and Materials, May 20-22, 2020, Brno, Czech Republic. [S.l.]: TANGER Ltd., 2020: 1037-1041.

[98] Gussone J, Hagedorn Y C, Gherekhloo H, et al. Microstructure of γ-titanium aluminide processed by selective laser melting at elevated temperatures[J]. Intermetallics, 2015, 66: 133-140.

[99] Deng H, Qiu W B, Chen L Q, et al. Microstructure and mechanical property of Ti-5Al-5Mo-5V-3Cr-1Zr alloy fabricated by selective laser melting with a preheated substrate[J]. Advanced Engineering Materials, 2021, 23(9): 2100265.

[100] Zhu S M, Katti I, Qiu D, et al. Microstructural analysis of the influences of platform preheating and post-build heat treatment on mechanical properties of laser powder bed fusion manufactured AlSi10Mg alloy[J]. Materials Science and Engineering: A, 2023, 882: 145486.

[101] Nezhadfar P D, Shamsaei N, Phan N. Enhancing ductility and fatigue strength of additively manufactured metallic materials by preheating the build platform[J]. Fatigue & Fracture of Engineering Materials & Structures, 2021, 44(1): 257-270.

[102] Liang J W, Wu S B, Lei Z L, et al. *In-situ* aging treatment by preheating to obtain high-strength ZK60 Mg alloy processed by laser powder bed fusion[J]. Materials Characterization, 2022, 194: 112361.

[103] Chen Y X, Wang W H, Ou Y, et al. Effect of high preheating on the microstructure and mechanical properties of high gamma prime Ni-based superalloy manufactured by laser powder bed fusion[J]. Journal of Alloys and Compounds, 2023, 960: 170598.

[104] Chambrin N, Dalverny O, Cloue J M, et al. *In situ* ageing with the platform preheating of AlSi10Mg alloy manufactured by laser powder-bed fusion process[J]. Metals, 2022, 12(12): 2148.

[105] Krajňák T, Janeček M, Kozlik J, et al. Influence of the thermal history on the phase composition of laser directed energy deposited Ti-8.5wt% Mo alloy[J]. Materials & Design, 2022, 222: 111049.

[106] Cui C, Leitner H, Platl J, et al. Influence of platform preheating on *in situ* precipitation in an FeCoMo alloy during laser powder bed fusion[J]. Materials Characterization, 2023, 197: 112689.

[107] Ali H, Ma L, Ghadbeigi H, et al. *In-situ* residual stress reduction, martensitic decomposition and mechanical properties enhancement through high temperature powder bed pre-heating of selective laser melted Ti6Al4V[J]. Materials Science and Engineering: A, 2017, 695: 211-220.

[108] Baek G Y, Lee K Y, Park S H, et al. Effects of substrate preheating during direct energy deposition on microstructure, hardness, tensile strength, and notch toughness[J]. Metals and Materials International, 2017, 23(6): 1204-1215.

[109] Zhou L B, Sun J S, Chen J, et al. Study of substrate preheating on the microstructure and mechanical performance of Ti-15Mo alloy processed by selective laser melting[J]. Journal of Alloys and Compounds, 2022, 928: 167130.

[110] Mertens R, Dadbakhsh S, van Humbeeck J, et al. Application of base plate preheating during selective laser melting[J]. Procedia CIRP, 2018, 74: 5-11.

[111] Müller A V, Schlick G, Neu R, et al. Additive manufacturing of pure tungsten by means of selective laser beam melting with substrate preheating temperatures up to 1000 ℃[J]. Nuclear Materials and Energy, 2019, 19: 184-188.

[112] Li W, Liu J, Zhou Y, et al. Effect of substrate preheating on the texture, phase and nanohardness of a Ti-45Al-2Cr-5Nb alloy processed by selective laser melting[J]. Scripta Materialia, 2016, 118: 13-18.

[113] Shim D S, Baek G Y, Lee E M. Effect of substrate preheating by induction heater on direct energy deposition of AISI M4 powder[J]. Materials Science and Engineering: A, 2017, 682: 550-562.

[114] Caprio L, Demir A G, Chiari G, et al. Defect-free laser powder bed fusion of Ti-48Al-2Cr-2Nb with a high temperature inductive preheating system[J]. Journal of Physics: Photonics, 2020, 2(2): 024001.

[115] Dalaee M T, Gloor L, Leinenbach C, et al. Experimental and numerical study of the influence of induction heating process on build rates induction heating-assisted laser direct metal deposition (IH-DMD) [J]. Surface and Coatings Technology, 2020, 384: 125275.

[116] Fan W, Tan H, Zhang F Y, et al. Effect of synchronous induction heating on residual stress for laser-based directed energy deposition of thin-walled structures[J]. Materials Today Communications, 2023, 35: 105702.

[117] Papadakis L, Chantzis D, Salonitis K. On the energy efficiency of pre-heating methods in SLM/SLS processes[J]. The International Journal of Advanced Manufacturing Technology, 2018, 95(1): 1325-1338.

[118] Yan L, Zhang Y L, Liou F. A conceptual design of residual stress reduction with multiple shape laser beams in direct laser deposition [J]. Finite Elements in Analysis and Design, 2018, 144: 30-37.

[119] Meng W, Zhang W H, Zhang W, et al. Additive fabrication of 316L/Inconel625/Ti6Al4V functionally graded materials by laser synchronous preheating[J]. The International Journal of Advanced Manufacturing Technology, 2019, 104(5): 2525-2538.

[120] Wei M, Yin X H, Wang Z, et al. Additive manufacturing of a functionally graded material from Inconel625 to Ti6Al4V by laser synchronous preheating[J]. Journal of Materials Processing Technology, 2020, 275: 116368.

[121] Meng W, Zhang W H, Zhang W, et al. Fabrication of steel-Inconel functionally graded materials by laser melting deposition integrating with laser synchronous preheating[J]. Optics Laser Technology, 2020, 131: 106451.

[122] Chen C P, Xiao Z X, Wang Y L, et al. Prediction study on *in situ* reduction of thermal stress using combined laser beams in laser powder bed fusion[J]. Additive Manufacturing, 2021, 47: 102221.

[123] Maurya H S, Kosiba K, Juhani K, et al. Effect of powder bed preheating on the crack formation and microstructure in ceramic matrix composites fabricated by laser powder-bed fusion process[J]. Additive Manufacturing, 2022, 58: 103013.

[124] Zhang W Y, Abbott W M, Sasnauskas A, et al. Process parameters optimisation for mitigating residual stress in dual-laser beam powder bed fusion additive manufacturing[J]. Metals, 2022, 12(3): 420.

[125] Li X, Gagnoud A, Ren Z M, et al. Investigation of thermoelectric magnetic convection and its effect on solidification structure during directional solidification under a low axial magnetic field[J]. Acta Materialia, 2009, 57(7): 2180-2197.

[126] Li X, Fautrelle Y, Gagnoud A, et al. Effect of a weak transverse magnetic field on solidification structure during directional solidification[J]. Acta Materialia, 2014, 64: 367-381.

[127] Xu W, Surla V, Jaworski M A, et al. Investigation of the heat transfer in TEMHD driven swirling lithium flow[J]. Journal of Nuclear Materials, 2011, 415(1): S981-S984.

[128] Du D F, Wang L, Dong A P, et al. Promoting the densification and grain refinement with assistance of static magnetic field in laser powder bed fusion[J]. International Journal of Machine Tools and Manufacture, 2022, 183: 103965.

[129] Wang L, Yan W T. Thermoelectric magnetohydrodynamic model for laser-based metal additive manufacturing[J]. Physical Review Applied, 2021, 15(6): 064051.

[130] Zhou H X, Song C H, Yang Y Q, et al. Effect of axial static magnetic field on microstructure evolution, performance, and melt pool signals of AlSi10Mg fabricated by laser powder bed fusion[J]. Optics Laser Technology, 2023, 163: 109316.

[131] Kang N, Yuan H, Coddet P, et al. On the texture, phase and tensile properties of commercially pure Ti produced via selective laser melting assisted by static magnetic field[J]. Materials Science & Engineering C, Materials for Biological Applications, 2017, 70(1): 405-407.

[132] Zhu W L, Yu S, Chen C Y, et al. Effects of static magnetic field on the microstructure of selective laser melted Inconel 625 superalloy: numerical and experiment investigations[J]. Metals, 2021, 11(11): 1846.

[133] Du D F, Haley J C, Dong A P, et al. Influence of static magnetic field on microstructure and mechanical behavior of selective laser melted AlSi10Mg alloy[J]. Materials & Design, 2019, 181: 107923.

[134] Nie J W, Chen C Y, Shuai S S, et al. Effect of static magnetic field on the evolution of residual stress and microstructure of laser remelted Inconel 718 superalloy[J]. Journal of Thermal Spray Technology, 2020, 29(6): 1410-1423.

[135] Wang R, Wang J, Lei L M, et al. Laser additive manufacturing of strong and ductile Al-12Si alloy under static magnetic field[J]. Journal of Materials Science & Technology, 2023, 163: 101-112.

[136] Filimonov A M, Rogozin O A, Dubinin O N, et al. Modification of mechanical properties in directed energy deposition by a static magnetic field: experimental and theoretical analysis[J]. Materials, 2021, 14(18): 5190.

[137] Chen L W, Li H, Liu S, et al. Simulation of surface deformation control during selective laser melting of AlSi10Mg powder using an external magnetic field[J]. AIP Advances, 2019, 9(4): 045012.

[138] Bian Q F, Tang X L, Dai R K, et al. Evolution phenomena and surface shrink of the melt pool in an additive manufacturing process under magnetic field[J]. International Journal of Heat and Mass Transfer, 2018, 123: 760-775.

[139] Fan X Q, Fleming T G, Rees D T, et al. Thermoelectric magnetohydrodynamic control of melt pool flow during laser directed energy deposition additive manufacturing[J]. Additive Manufacturing, 2023, 71: 103587.

[140] Zhao R X, Chen C Y, Shuai S S, et al. Enhanced mechanical properties of Ti6Al4V alloy fabricated by laser additive manufacturing under static magnetic field[J]. Materials Research Letters, 2022, 10(8): 530-538.

[141] Smith P H, Murray J W, Jones D O, et al. Magnetically assisted directed energy deposition[J]. Journal of Materials Processing Technology, 2021, 288: 116892.

[142] Smith P H, Murray J W, Jackson-Crisp A, et al. Magnetic manipulation in directed energy deposition using a programmable solenoid[J]. Journal of Materials Processing Technology, 2022, 299: 117342.

[143] Zhou H X, Song C H, Yang Y Q, et al. The microstructure and properties evolution of SS316L fabricated by magnetic field-assisted laser powder bed fusion[J]. Materials Science and Engineering: A, 2022, 845: 143216.

[144] Ma G Y, Liu X, Song C C, et al. TiCp reinforced Ti6Al4V of follow-up synchronous electromagnetic induction-laser hybrid directed energy deposition: microstructure evolution and mechanical properties[J]. Additive Manufacturing, 2022, 59: 103087.

[145] Zheng Y, Cao L, Wang J, et al. Surface morphology refinement and Laves phase control of plasma arc additively manufactured Inconel 718 via an alternating magnetic field[J]. Materials & Design, 2022, 223: 111161.

[146] 俞启东, 徐志程, 赵静, 等. 超声空化及其声流结构实验研究[J]. 应用声学, 2021, 40(6): 865-870.
Yu Q D, Xu Z C, Zhao J, et al. Experimental study on ultrasonic cavitation and acoustic streaming structure[J]. Journal of Applied Acoustics, 2021, 40(6): 865-870.

[147] Guo A F, Tang R J, Guo S, et al. Acoustic field-assisted powder bed fusion of tungsten carbide-reinforced 316L stainless steel composites[J]. Journal of Materials Research and Technology, 2023, 26: 5488-5502.

[148] Yan Z W, Trofimov V, Song C H, et al. Microstructure and mechanical properties of GH5188 superalloy additively

manufactured via ultrasonic-assisted laser powder bed fusion[J]. Journal of Alloys and Compounds, 2023, 939: 168771.
[149] Cong W L, Ning F D. A fundamental investigation on ultrasonic vibration-assisted laser engineered net shaping of stainless steel[J]. International Journal of Machine Tools and Manufacture, 2017, 121: 61-69.
[150] Niu F Y, Li Y, Song C C, et al. Microstructure and wear resistance of TiCp/Ti6Al4V composite coatings by follow-up ultrasonic-assisted laser additive manufacturing[J]. Coatings, 2022, 12(7): 986.
[151] Wu D J, Song C C, Di T D, et al. Intermetallic regulation mechanism of Inconel 718/Ti6Al4V composite by novel follow-up ultrasonic assisted laser additive manufacturing[J]. Composites Part B: Engineering, 2022, 235: 109736.
[152] Gorunov A I. Additive manufacturing of Ti6Al4V parts using ultrasonic assisted direct energy deposition[J]. Journal of Manufacturing Processes, 2020, 59: 545-556.
[153] Wang H, Hu Y B, Ning F D, et al. Ultrasonic vibration-assisted laser engineered net shaping of Inconel 718 parts: effects of ultrasonic frequency on microstructural and mechanical properties [J]. Journal of Materials Processing Technology, 2020, 276: 116395.
[154] Todaro C J, Easton M A, Qiu D, et al. Grain refinement of stainless steel in ultrasound-assisted additive manufacturing[J]. Additive Manufacturing, 2021, 37: 101632.
[155] Chen Y J, Zhou Q. Directed energy deposition additive manufacturing of CoCrFeMnNi high-entropy alloy towards densification, grain structure control and improved tensile properties[J]. Materials Science and Engineering: A, 2022, 860: 144272.
[156] Yao Z H, Wang Z, Chen J, et al. Equiaxed microstructure formation by ultrasonic assisted laser metal deposition[J]. Manufacturing Letters, 2022, 31: 56-59.
[157] 孙徕博, 黄陆军, 黄瑞生, 等. 超声冲击对增材制造组织改善及强化机理影响的研究进展[J]. 金属学报, 2024, 60(3): 273-286.
Sun L B, Huang L J, Huang R S, et al. Progress in the effect of ultrasonic impact treatment on microstructure improvement and strengthening mechanism in additive manufacturing[J]. Acta Metallurgica Sinica, 2024, 60(3): 273-286.
[158] Zhang M X, Liu C M, Shi X Z, et al. Residual stress, defects and grain morphology of Ti-6Al-4V alloy produced by ultrasonic impact treatment assisted selective laser melting[J]. Applied Sciences, 2016, 6(11): 304.
[159] Wang Y C, Roy S, Choi H, et al. Cracking suppression in additive manufacturing of hard-to-weld nickel-based superalloy through layer-wise ultrasonic impact peening[J]. Journal of Manufacturing Processes, 2022, 80: 320-327.
[160] Zhou C P, Wang J D, Guo C H, et al. Numerical study of the ultrasonic impact on additive manufactured parts[J]. International Journal of Mechanical Sciences, 2021, 197: 106334.
[161] Wang F B, Liu Y K, Zhang B B, et al. Strengthening effect in laser metal deposited Ti6Al4V alloy via layer-by-layer ultrasonic impact treatment[J]. Materials Science and Engineering: A, 2023, 886: 145693.
[162] Wang Y C, Shi J. Microstructure and properties of Inconel 718 fabricated by directed energy deposition with *in-situ* ultrasonic impact peening[J]. Metallurgical and Materials Transactions B, 2019, 50(6): 2815-2827.
[163] Xu L Y, Gao Y L, Zhao L, et al. Ultrasonic micro-forging post-treatment assisted laser directed energy deposition approach to manufacture high-strength Hastelloy X superalloy[J]. Journal of Materials Processing Technology, 2022, 299: 117324.
[164] Wei X, Li X L, Zhang L Q, et al. Effect of *in situ* ultrasonic impact treatment on flow and solidification behavior of laser metal deposition: by finite element simulation[J]. International Journal of Heat and Mass Transfer, 2022, 192: 122914.
[165] Wang Y C, Shi J. Recrystallization behavior and tensile properties of laser metal deposited Inconel 718 upon *in situ* ultrasonic impact peening and heat treatment[J]. Materials Science and Engineering: A, 2020, 786: 139434.

Research Status and Prospect of Multi-Field Modulated Metal Laser Additive Manufacturing

Gao Hairui, Li Jikang, Zhang Zhenwu, Zheng Keying, Xiang Honghao, Wei Qingsong*
School of Materials Science and Engineering, Huazhong University of Science and Technology, Wuhan 430074, *Hubei, China*

Abstract

Significance Laser additive manufacturing (LAM) technology uses a focused high-energy laser beam as the heat source to achieve integrated forming of complex metal components, avoiding the complex post-processing steps of traditional processing techniques and achieving high forming efficiency, which makes it have broad application prospects in aerospace, automotive, medical and other fields. The metal additive manufacturing process based on laser and powder mainly includes two types: selective laser melting (SLM) and laser directed energy deposition (LDED). LAM has been widely used in the forming of various metal materials, including aluminum alloys, titanium alloys, copper alloys, nickel-based superalloys, magnesium alloys, steel, and so on.

Due to the current widespread use of Gaussian laser in laser additive manufacturing technology, the peak intensity generated in the focusing area is very high. When laser interacts with metal powder, the width-to-depth ratio of the melt pool is small and there are large temperature gradient and cooling rate. The instability caused by complex melt flow dynamics and the accumulation of repeated heating and cooling cycles are prone to keyholes, splashing, spheroidization, residual stress, cracks, and anisotropic microstructures, which seriously affect the strength, toughness, and fatigue resistance of formed components in turn. Modifying the alloy composition

or adding strengthening phase particles can effectively eliminate the cracks and anisotropic columnar crystal structure in metal samples. It should be noted that component modification may cause pitting corrosion and reduce the corrosion resistance of the alloy, and the addition of strengthening phase particles to the alloy may lead to particle agglomeration and poor bonding between the strengthening phase and the matrix interface. Heat treatment is an effective method to eliminate cracks and defects in LAM-prepared samples. However, heat treatment further prolongs the preparation time and increases the complexity of the forming process.

Laser shaping and external field matching can regulate the LAM process from the source, solving the problem of defects in formed components. Revealing the *in-situ* function mechanism and influence law of organization and performance between laser/thermal/magnetic/acoustic fields and materials provides reference for future research on metal LAM technology, promoting its widespread application in multiple fields.

Progress The distribution of laser energy can affect the spatial shape of the melt pool, thereby affecting the thermal gradient and metal cooling and solidification process. Flat-top laser, anti-Gaussian laser, Bessel laser, and defocusing laser all weaken the peak energy in the center of the traditional Gaussian laser beam to different degrees, reduce the temperature gradient in melt pool, suppress powder evaporation and splashing, limit the keyhole effect, and thus reduce the number of defects such as pores and cracks within a wider process window, obtaining almost dense samples. From the perspective of the influence on grain orientation, flat-top laser, anti-Gaussian laser, and defocusing laser can increase the width-to-depth ratio of the melt pool, and research has shown that they can promote the epitaxial growth of columnar crystals. Especially, flat-top laser has a uniform energy distribution, which can obtain almost complete <001> oriented textures, which is beneficial for the preparation of single crystals and β-type medical titanium alloys. In contrast, the elliptical beam profile has a significant impact on the solidification microstructure. By reducing the temperature gradient of the melt pool and increasing the undercooling zone of the composition, the nucleation tendency is improved. It is beneficial for equiaxed crystal formation and achieving grain refinement and tissue densification.

The thermal field reduces the temperature gradient of the melt pool during LAM through heat transfer, prolongs the solidification time of the melt pool, reduces element segregation, and eliminates residual stress and cracks in formed components. The thermal field formed by substrate preheating is gradually transmitted to the surface of the formed part through contact from bottom to top. The process is simple, but it can cause uneven microstructure and properties of the formed component along the building direction. Moreover, due to the high integration of LAM equipment, it is difficult to achieve high preheating temperature. Electromagnetic induction heating can uniformly preheat the entire formed component, avoiding tissue anisotropy caused by uneven preheating, and can achieve high preheating temperature. However, the process is complex and puts forward high requirements for LAM equipment. The static and alternating magnetic field-assisted metal LAM technology has proven to have excellent effects on different forming materials. By generating Lorentz forces and thermoelectric convection to regulate the flow of molten metal in the melt pool, grain refinement is achieved, isotropic equiaxed crystal zone formation is promoted, harmful phase precipitation is suppressed, and mechanical properties are improved. In the process of ultrasonic assisted LAM, the acoustic flow effect can promote the uniform distribution of solutes in the melt pool and reduce segregation. Cavitation effect causes dendrite fragmentation to increase nucleation sites, which promotes grain refinement and epitaxial to equiaxed transformation, and improves the mechanical properties of the prepared samples. In addition, ultrasonic fields can also alleviate residual stresses in formed samples and suppress the generation of defects such as cracks.

Conclusions and Prospects Research at home and abroad has confirmed that laser shaping and thermal/magnetic/ultrasonic fields can regulate the shape of the melt pool and the cooling solidification process *in situ* during the forming process, so as to overcome the defects that affect the quality of formed parts in metal LAM technology. The mechanism of action of different forms of fields on the solidification process of melt pool metal is different. In the future, further exploration can focus on the effect of multi-field synchronously assisted LAM technology on different forming materials, and broaden the application prospects of metal LAM technology in different fields.

Key words laser technique; laser additive manufacturing; beam shaping; magnetic field; thermal field; ultrasonic field